AD-A067 916 VARIAN ASSOCIATES INC PALO ALTO CA F/G 9/1
AN INVESTIGATION OF POWER SUCK-OUT IN HELIX TRAVELING-WAVE TUBE--ETC(U)
DEC 78 D P HINSON F49620-77-C-0102
UNCLASSIFIED AFOSR-TR-79-0392 NL

1 OF 2
ADA
067916

AFOSR-TR- 79-0392

LEVEL

3

AD A067916

DDC FILE COPY

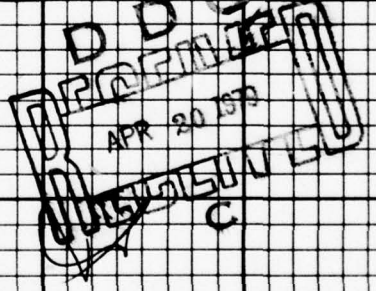

WATKINS-JOHNSON

79 04 13 012

Approved for public release; distribution unlimited.

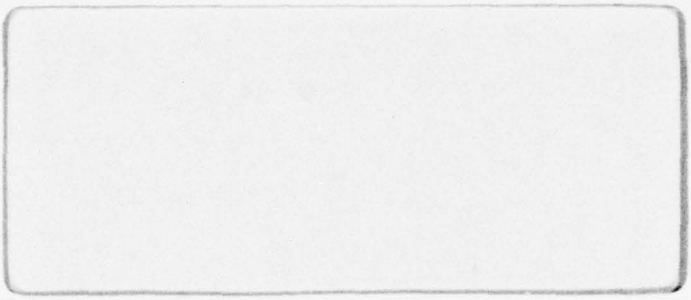

AIR FORCE OFFICE OF SCIENTIFIC RESEARCH (AFSC)
NOTICE OF TRANSMITTAL TO DDC
This technical report has been reviewed and is approved for public release IAW AFR 190-12 (7b).
Distribution is unlimited.
A. D. BLOSE
Technical Information Officer

3

AN INVESTIGATION OF POWER SUCK-OUT IN HELIX TRAVELING-WAVE TUBES

A THESIS

SUBMITTED TO THE DEPARTMENT OF ELECTRICAL ENGINEERING

AND THE COMMITTEE ON GRADUATE STUDIES

OF STANFORD UNIVERSITY

IN PARTIAL FULFILLMENT OF THE REQUIREMENTS

FOR THE DEGREE OF

ENGINEER

By

David Pryor Hinson

December 1978

UNCLASSIFIED
SECURITY CLASSIFICATION OF THIS PAGE (When Data Entered)

REPORT DOCUMENTATION PAGE	READ INSTRUCTIONS BEFORE COMPLETING FORM
1. REPORT NUMBER: AFOSR-TR-79-0392	2. GOVT ACCESSION NO. / 3. RECIPIENT'S CATALOG NUMBER
4. TITLE (and Subtitle): An Investigation of Power Suck-out in Helix Traveling-wave Tubes,	5. TYPE OF REPORT & PERIOD COVERED: Final / Rept. / 6. PERFORMING ORG. REPORT NUMBER
7. AUTHOR(s): David Pryor Hinson	8. CONTRACT OR GRANT NUMBER(s): F49620-77-C-0102
9. PERFORMING ORGANIZATION NAME AND ADDRESS: Varian Associates, 611 Hansen Way, Palo Alto, California 94303	10. PROGRAM ELEMENT, PROJECT, TASK AREA & WORK UNIT NUMBERS: 2305/C1, 61102F
11. CONTROLLING OFFICE NAME AND ADDRESS: AFOSR/NE, Directorate of Electronic and Solid State Sciences, Bldg #410, Bolling AFB, DC 20332	12. REPORT DATE: December 1978 / 13. NUMBER OF PAGES: 97
14. MONITORING AGENCY NAME & ADDRESS (if different from Controlling Office): 99p.	15. SECURITY CLASS. (of this report): UNCLASSIFIED / 15a. DECLASSIFICATION/DOWNGRADING SCHEDULE

16. DISTRIBUTION STATEMENT (of this Report)

"Approved for public release; distribution unlimited."

17. DISTRIBUTION STATEMENT (of the abstract entered in Block 20, if different from Report)

18. SUPPLEMENTARY NOTES

19. KEY WORDS (Continue on reverse side if necessary and identify by block number)

20. ABSTRACT (Continue on reverse side if necessary and identify by block number)

This report describes the results of an experimental investigation of power suck-out in high power single helix traveling-wave amplifiers. The objective here is to perform a variety of measurements which thoroughly and systematically characterize the phenomenon in one particular tube type. The resulting description of power suck-out provides a firm basis for a theoretical solution, and indicates design considerations which may reduce its effects. In particular, the results establish a relationship between the power holes and the output helix stop band at pi radians phase shift per helix turn, and suggest an interpretation of the

other side

DD FORM 1 JAN 73 1473 EDITION OF 1 NOV 65 IS OBSOLETE

364 100

UNCLASSIFIED

Approved for the Department:

Marvin Chodorow

Approved for the University Committee
on Graduate Studies:

W T Carnochan

Contract no. F49620-77-C-0102 Varian assoc.

Acknowledgments

I wish to gratefully acknowledge the support of the Air Force After Program in funding this research. All experimental work was conducted at Watkins-Johnson Company with considerable assistance from the engineers and technicians there. A special thanks to Dr. D.J. Bates of W.J. and Dr. M. Chodorow of Stanford for their supervision which made this thesis possible.

CONTENTS

I. INTRODUCTION

In the operation of traveling-wave and magnetron type microwave amplifiers, cumulative interaction occurs when the electron beam travels in near synchronism with an electromagnetic wave. But phase velocities associated with ordinary waveguides exceed the velocity of light, while electron velocities cannot. Therefore, specialized slow wave structures, capable of propagating electromagnetic waves with phase velocities less than the velocity of light, are required for useful interaction with electron beams. Typical examples include the helix supported by dielectric rods, the meander line used in injected beam crossed-field amplifiers (IBCFA'S), the periodically loaded (slotted ridge) waveguide, and the coupled cavity structure.

Associated with the Brillouin diagrams[1] (ω vs. β) of each of these structures are frequencies where the group velocity approaches zero for the various modes of propagation. For example, this feature appears in the ω-β diagrams of the periodically loaded waveguide derived by Gewartowski and Watson[2], and the coupled cavity structure analyzed by Gittins[3]. In both these cases, the regions of low group velocity arise from the band pass behavior of the slow wave circuits. Alternatively, stop bands which are not theoretical characteristics of a particular ideal slow wave structure may result from imperfections in construction. These stop bands introduce additional frequency regions of low group velocity.

The regions of low group velocity and resultant high interaction

impedance can cause undesirable effects in amplifier behavior. Drive induced oscillations occur near the upper pass band frequency, where group velocity nears zero, in coupled cavity traveling-wave amplifiers. G. Dohler and R. Moats[4] are presently investigating "parametric oscillations" in IBCFA's associated with a stop band at pi radians phase shift per bar in the meander line slow wave circuit. These two examples involve regions of low group velocity which are characteristic of the slow wave structures. In high power single helix traveling-wave amplifiers, a stop band may appear at the (0) and (-1) space harmonic crossover frequency, corresponding to pi radians phase shift per helix turn. This is not a theoretical characterisitc of the slow wave structure, but results from multiple periodicities and asymmetries which are introduced by imperfections in tube construction. A type of power hole apparently associated with this stop band repeatedly appears at one half the crossover frequency.

While most researchers in the field periodically encounter this type of power hole, and a number of explanations have been proposed, the phenomenon has never been systematically investigated or explained theoretically in a satisfactory manner. The following observations concerning this phenomenon, alternatively referred to as power suck-out, derive from an unpublished memorandum written by L.M. Winslow of N.R.L., and private discussions with D.J. Bates and M.V. Purnell of Watkins-Johnson company. These characteristics comprise the description of power suck-out preceding this report:

a) power suck-out commonly occurs at high cathode currents

in dual mode tubes, with single mode tubes seldom affected;

b) two power holes appear at adjacent frequencies, with each approximately 30 MHz wide and up to 10 db in depth (these two quantities vary between TWT's);

c) the power holes appear at approximately one half the (0) and (-1) space harmonic crossover frequency;

d) the depth of each power hole depends on cathode current, helix voltage, and input power level;

e) at low input signal levels the power holes are imperceptible; they occur only at large signals implying that harmonic content of the beam current may be important;

f) the power holes are most severe near saturated output power;

g) the output power absent at the fundamental frequency does not appear at the second harmonic;

h) other observations and speculations have been made prior to this report, but none which were soundly experimentally supported to the knowledge of this author.

Figure 1 displays the typical appearance of the phenomenon. The observation dates from June, 1975 and shows fundamental output power vs. frequency (within the operating band of the tube) 3 db below saturation. Because the power holes appear at saturation, power suck-out places severe limitations on dual mode amplifier operation within design specifications. And preliminary measurements in this study revealed that a suitable adjustment of helix voltage accompanied by an increase in cathode current produced power suck-out in five of the six dual mode tubes investigated.

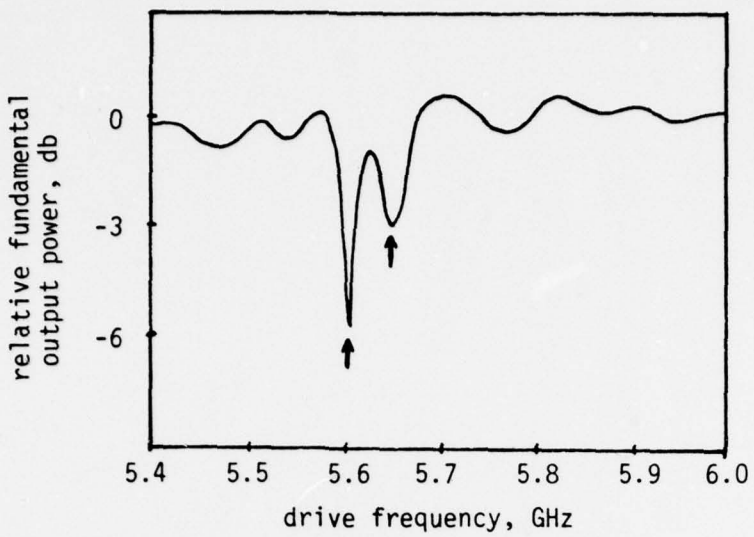

Figure 1. Fundamental output power vs. drive frequency for constant input power. Output power is 3 db below saturation. Helix voltage is 8000 volts; cathode current is 0.600 amps. Power holes are indicated by arrows: frequency of deeper hole is 5.61 GHz, depth of deeper hole is 6.0 db.

With this background, this report describes the results of an experimental investigation of power suck-out in high power single helix traveling-wave amplifiers. The objective here is to perform a variety of measurements which thoroughly and systematically characterize the phenomenon in one particular tube type. The resulting description of power suck-out provides a firm basis for a theoretical solution, and indicates design considerations which may reduce its effects. In particular, the results establish a relationship between the power holes and the output helix stop band at pi radians phase shift per helix turn, and suggest an interpretation of the interaction which causes power suck-out.

The report is organized as follows. Section II presents a theoretical model for the stop band which appears at pi radians

phase shift per helix turn. With emphasis on systematic presentation of data, section III describes results of experiments involving power suck-out as it appears in Watkins-Johnson traveling-wave amplifiers. Section IV summarizes the results of section III and discusses a plausible qualitative explanation for the phenomenon. Section V contains recommendations for further research and indicates implications of the results on amplifier design. A summary of the experimental methods and equipment used in this study appears in an appendix.

II. THE HELIX STOP BAND

This section presents a theoretical model which predicts certain important characteristics of the stop band present at pi radians phase shift per helix turn.

Two space harmonics of the Brillouin diagram for a lossless helix in free space appear in figure 2*.

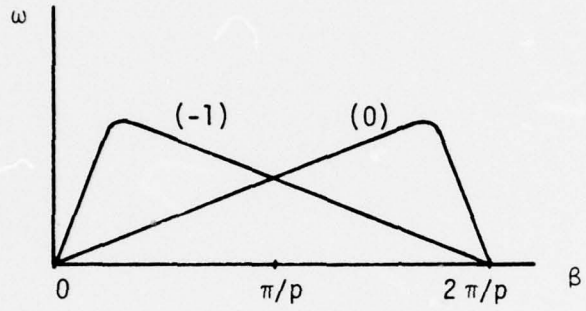

ω = angular frequency
β = wavenumber measured along the helix axis
p = axial distance between helix turns

Figure 2. Two space harmonics of the Brillouin diagram for a lossless helix in free space.

Broadband traveling-wave amplification relies on properties of the (0) space harmonic, while backward wave oscillation involves the (-1) space harmonic. No means of coupling energy between waves with forward and backward group velocity exists for this idealized helix structure. In actual traveling-wave amplifiers, dielectric rods support the helix inside a conducting cylindrical sleeve as shown in figure 3. The abrupt discontinuity presented by the rods causes reflections, allowing interaction between waves with forward and backward group velocity. And any misalignment of dielectric rods in rf circuit construction influences the coupling.

*The reader is referred to Sensiper's[5] rigorous treatment of propagation on helical structures for more detailed information.

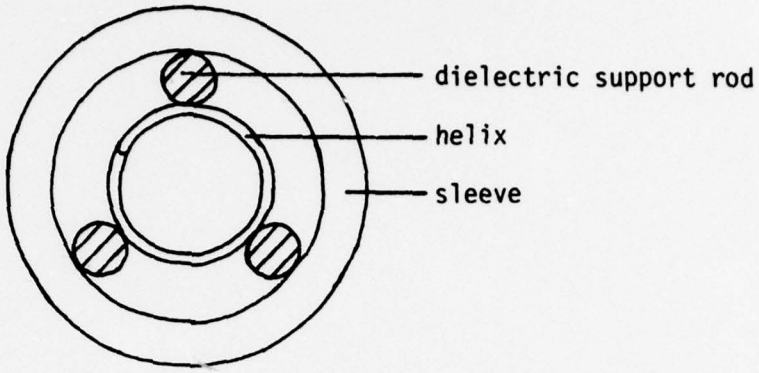

Figure 3. End view of helix structure.

To develop a simple model for the coupling, note that in the frequency range of interest for the (0) space harmonic, the electromagnetic wave propagates roughly in a 'TEM' mode at the velocity of light, c, along the helix wire.[5,6] This is consistent with the observed nearly constant phase velocity of $c/\cot \psi$ along the helix axis at these frequencies, where ψ is the helix pitch angle. At each point in its progression along the wire where the wave encounters a support rod, part of the energy is reflected with the rest transmitted. The phase relationship of successive reflections determines to what extent the support rods disturb ideal propagation and introduce frequency dependent coupling between forward and backward waves.

Consider helix excitation at the frequency where $\beta = \pi/p$, the crossover point of the two space harmonics of figure 2. For a helix supported by three perfectly aligned rods, reflections from successive junctions of helix wire with dielectric rod are 120° out of phase. Consequently, assuming that the reflection coefficient associated with each junction is very small, in accordance with

good tube design*, the reflections add to zero and there is no coupling between forward and backward waves at this frequency. As might be expected from this observation, application of coupled mode theory within this simple model shows that perfectly aligned dielectric rods do not introduce a stop band at the crossover frequency, as will subsequently be shown.

The effect of misaligned support rods can be evaluated within this framework. Actually, a number of imperfections in rf circuit construction, such as nonsymmetric attenuation on support rods, slots in the helix sleeve, periodic variations in helix pitch, or changes in helix shape due to strain, introduce asymmetries and multiple periodicities which contribute to coupling between forward and backward waves. These mechanisms combine and lead to coupling which is spatially varying. For simplicity only the effect of misaligned support rods is considered; furthermore, the coupling is assumed to be continuous. In the region of the crossover in figure 2, equations for the two space harmonics in the absence of coupling can be approximated as

$$\begin{aligned} \beta_+ &= \frac{\omega}{c} \cot \psi \\ \beta_- &= \frac{2\pi}{p} - \frac{\omega}{c} \cot \psi \end{aligned} \tag{1}$$

Pierce's coupled mode theory[6,7] (assuming continuous coupling) then predicts that with the addition of coupling we now have

$$\beta_{1,2} = \frac{\beta_+ + \beta_-}{2} \pm \left[\left(\frac{\beta_+ - \beta_-}{2} \right)^2 - K^2 \right]^{1/2} \tag{2}$$

*Materials chosen for support rods are characterized by a low relative dielectric constant; this minimizes their effect on helix propagation.

The coupling factor, K, must be evaluated from a model describing the helix and support structure.

A helix length of one turn and its three junctions of helix

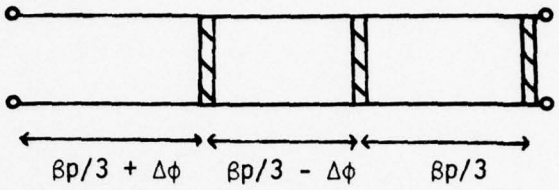

Figure 4.

wire with dielectric support rod are shown schematically in figure 4. For perfectly aligned rods, the phase separation of the junctions is $\beta p/3$; note that one junction is displaced by an angle $\Delta\phi$, corresponding to one rod misaligned by this amount. If the reflection coefficient of one junction, ρ_0, is assumed to be very small, the three reflections from a normalized wave incident from the left add approximately as follows:

$$R \simeq \rho_0\{\exp j(\tfrac{-2\beta p}{3} - 2\Delta\phi) + \exp j(\tfrac{-4\beta p}{3}) + \exp j(-2\beta p)\} \qquad (3)$$

where R is defined as the total reflection from this helix section, and terms of second order in ρ_0 are neglected. To determine the effect of coupling near the crossover frequency, we define

$$\beta p = \pi + \theta \qquad (4)$$

and assume that θ and $\Delta\phi$ are both small. Then, to first order in the small quantities:

$$R \simeq \rho_0\{(\tfrac{\theta}{\sqrt{3}} - \sqrt{3}\Delta\phi) - j(\theta - \Delta\phi)\} \qquad (5)$$

It is clear that perfectly aligned rods ($\Delta\phi=0$) do not introduce

coupling at the crossover frequency (θ=0), as stated previously. To evaluate K, the continuous coupling coefficient, we approximate:

$$K \simeq \frac{|R|}{p} \simeq \frac{|\rho_0|}{p}\left(\frac{4}{3}\theta^2 - 4\theta\Delta\phi + 4\Delta\phi^2 \right)^{1/2} \qquad (6)$$

as discussed by Watkins[6], where we assume that $|R|<<1$.

We can now evaluate the effects of misaligned support rods in the coupled mode theory. Substitution of equation (1) into (2) shows that the stop band appears as in figure 5, with:

$$\beta_{1,2} = \frac{\pi}{p} \pm \left\{ \left(\frac{\omega}{c}\cot\psi - \frac{\pi}{p} \right)^2 - K^2 \right\}^{1/2} \qquad (7)$$

The boundaries of the stop band are defined as those frequencies where the second term in equation (7) vanishes at θ=0 ($\beta=\frac{\pi}{p}$).

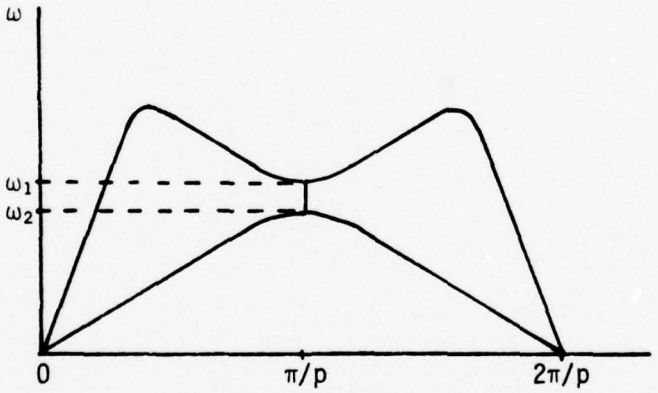

Figure 5. Appearance of the stop band on a lossless helix structure. The width of the stop band, $\omega_1 - \omega_2$, is exaggerated.

With this definition, the width of the stop band follows from equations (6) and (7):

$$\omega_1 - \omega_2 = \frac{4\,\Delta\phi\,|\rho_0|\,c}{p\,\cot\psi} \qquad (8a)$$

or:

$$\frac{\omega_1 - \omega_2}{\omega} = \frac{4\,\Delta\phi\,|\rho_0|}{\pi} \tag{8b}$$

For "typical" values* ($\Delta\phi$=0.2 radians, $|\rho_0|$=0.025), $\frac{\omega_1 - \omega_2}{\omega} \simeq 1\%$. Equation (8) clearly shows that perfectly aligned rods ($\Delta\phi$=0) do not introduce a stop band at the cross-over frequency, as stated earlier. Within the stop band, β has an imaginary part, given by

$$\mathrm{Im}(\beta_{1,2}) = \pm\left\{ \left|\frac{\rho_0}{p^2}\right|^2 4\Delta\phi^2 - \left(\frac{\omega}{c}\cot\psi - \frac{\pi}{p} \right)^2 \right\}^{1/2} \tag{9}$$

This imaginary part results entirely from the reflections which couple forward and backward waves and not from losses. These results predicted by the coupled mode equations now need some interpretation.

Chodorow defines a proportionality between the amplitude of the electric field in the forward circuit wave, E_r, and the power in the wave, P_r, as

$$K_p = \frac{E_r^2}{2\,\beta_1^2\,P_r} \tag{10}$$

where β_1 is the cold circuit propagation constant. Since the rate of energy flow in the wave, P_r, is directly proportional to the circuit group velocity $\frac{d\omega}{d\beta}$, equation (10) shows that the interaction impedance (coupling impedance), K_p, is inversely proportional to this

*This model for the stop band considers only the effect of misaligned dielectric helix support rods. In an attempt to account for the other factors (mentioned previously) contributing to the stop band which are not contained in the model, a relatively large value is chosen for $\Delta\phi$.

quantity. As seen in figure 5, group velocity approaches zero at frequencies near the boundaries of the stop band, resulting in a high interaction impedance in these regions. And because the gain parameter, C, first suggested by Pierce[9] is defined by

$$C^3 = K_p/4\ R_0 \qquad (11)$$

where R_0 is the ratio of cathode current to helix voltage, this model predicts enhanced gain at frequencies near the boundaries of the stop band. Within the stop band, the propagation constant has an imaginary part given by equation (9). At these frequencies, a forward wave launched on the cold circuit attenuates with distance. Nevertheless, the possibility of amplification exists within the stop band, as discussed by Reutz[10]. These gain mechanisms in and around the stop band play an important role in the qualitative explanation of power suck-out proposed in section IV.

To appreciate the difficulty in detecting this type of stop band, consider a lossless helix structure of finite length. Because successive reflections from a misaligned support rod add in phase, this helix transmits only a fraction of the energy introduced onto it at at stop band frequencies, with the rest reflected back through the input. This accounts for the attenuation predicted by equation (9). But circuit losses reduce the magnitude of the reflection, hindering any attempt to locate the stop band by measuring this quantity. Furthermore, on a circuit with losses, the boundaries of the stop band are no longer distinct. This can be seen by considering figure 6*, which qualitatively

*A similar figure was derived previously by E. Lien.[11]

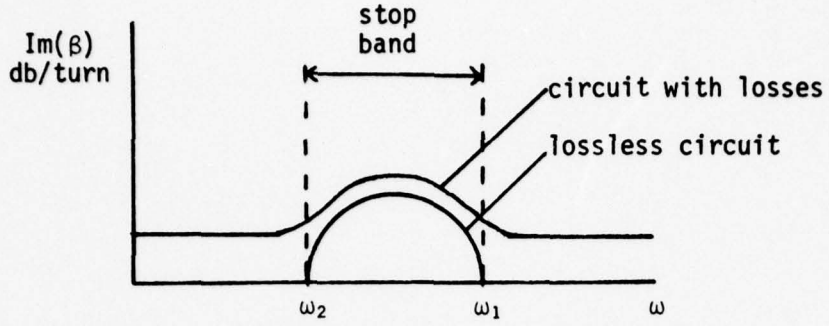

Figure 6. Imaginary part of β, corresponding to attenuation with distance along the helix axis, vs. frequency in the vicinity of the stop band.

displays the imaginary part of β, corresponding to attenuation with distance along the helix axis, both with and without circuit loss. In the former case, the stop band is dintinguished only by its increased attenuation over the value due to circuit losses alone, present at adjacent frequencies. Because of these difficulties, attempts at determining the presence and characteristics of such a stop band can produce inconclusive results.

III. MEASUREMENTS

Two Watkins-Johnson dual mode tube types were available for measurements concerning power suck-out. The developmental specifications of the WJ-3633-5 and WJ-3634-1 traveling-wave amplifiers appear below:

RF performance	WJ-3633-5	WJ-3634-1
frequency	2.6-5.2 GHz	4.8-9.6 GHz
rated output power*	400 watts pulsed	250 watts pulsed
	200 watts cw	125 watts cw
gain at rated power	40 db	28 db
Primary electrical requirements		
cathode voltage	-6.0 to -6.5 kV	-8.4 kV
cathode current	0.600 amps	0.450 amps
helix voltage	ground	ground
cathode to collector #1 voltage	4.7 kV	4.0 kV
collector #1 current	0.050 to 0.375 amps	0.050 to 0.350 amps
cathode to collector #2 voltage	1.8 kV	2.5 kV
collector #2 current	o.400 to 0.080 amps	0.400 to 0.100 amps
grid bias voltage (referenced to cathode)	-300. volts	-300. volts
grid drive voltage	140 volts	125 volts
filament voltage	6.3 volts	6.3 volts
filament current	2.7 amps	2.4 amps
focusing	ppm	ppm

Each tube employs a single helix with severs and dielectric support rods with lumped attenuation for oscillation suppression. More specific information involving such parameters as helix length or pitch will be provided as it becomes relevant.

Measurements on one particular WJ-3633-5 comprise most of the report. Power suck-out did not occur under best broadband operating conditions in this tube, but adjustment of helix voltage along with an increase in cathode current produced the phenomenon. Aside

*Dual mode operation.

from power suck-out, the device suffered no serious defects and was of production quality. This permitted performance of a wide variety of measurements to analyze the phenomenon as it affected normal amplification. Results of experiments performed on this tube appear in part A of section III. This data constitutes the experimental characterization of power suck-out undertaken in this study.

The limited availability of other operable tubes inhibited attempts to determine the generality of the results of section III.A. The only other functioning tubes found to be suitable for this study were two WJ-3634-1's. In these TWT's, power suck-out occured under optimum broadband operating conditions and therefore seriously degraded tube performance. Unfortunately, each displayed several other deviations from normal operation, along with power suck-out, which hampered measurements. But limited experiments designed to corroborate the observations of section III.A produced useful results which appear in part B of section III.

To avoid unnecessary diversion in this section, only a brief mention of apparatus appears where it is relevant. The appendix contains a detailed description of equipment used and the resulting limits of accuracy.

III.A. INVESTIGATION OF ONE WJ-3633-5 TWT

All data contained in section III.A derives from one specific WJ-3633-5 traveling wave amplifier. This section concentrates primarily on reporting the results of measurements, while the final interpretation of the data is postponed until section IV.

III.A.1 MEASUREMENT OF STOP BAND CHARACTERISTICS

The features of the stop band appearing at pi radians phase shift per helix turn were measured for both the input and output helix sections.* Subsequent investigation revealed a relationship between power suck-out and the output helix stop band, but no such connection to the input helix stop band. Therefore, the data concerning the input helix are omitted.

First, the frequency corresponding to pi radians phase shift per turn on the output helix was determined. Measurements of wavelength along the axis of the helix at discrete excitation frequencies produced the data points displayed in figure 7.

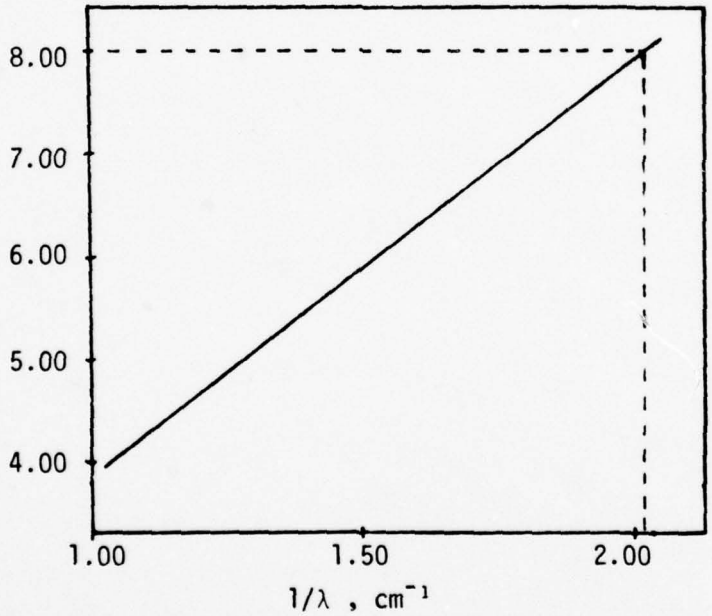

Figure 7. $1/\lambda$ vs. frequency on the (0) space harmonic for the output helix of the WJ-3633-5 TWT. The frequency corresponding to pi radians phase shift per helix turn is indicated. (The wavelength is measured along the axis of the helix.)

*These stop bands occur at different frequencies, since the two helices are wound with a different pitch.

The output helix section used for these measurements was identical to the one in the tube under investigation; its use eliminated the necessity of dismantling the operable TWT. For this helix, wound at 10.32 turns per inch, a phase shift of pi radians per helix turn occurs for $\beta = \frac{2\pi}{\lambda} = 12.76\ cm^{-1}$, or $1/\lambda = 2.03\ cm^{-1}$. From figure 7, the crossover frequency is therefore 8.00 GHz.

Let us briefly consider the effect produced by a stop band at the crossover frequency on TWT oscillations in the absense of input power. The frequency of oscillation depends on the frequency where the slow space charge wave line intersects the space harmonics shown in figure 5. However, since the stop band impedes energy propagation, oscillations at frequencies within the stop band will be suppressed. Therefore, as helix voltage is increased and the slow space charge wave line sweeps through the stop band region, we expect a rapid change in oscillation frequency from the value at the lower edge of the stop band to that at the upper edge of the stop band. Furthermore, any oscillation which occurs within the stop band will be characterized by a greater start current than is required at frequencies adjacent to the stop band.

Measurements of these oscillations indicate the presence of a stop band at the crossover frequency (8.00 GHz) on the output helix of the WJ-3633-5. At a particular helix voltage with no input signal, cathode current is increased until oscillation occurs on the output helix section. Measurements of the oscillation frequency and minimum beam current required for oscillation (start current) for various helix voltages appear in figures 8a and 8b.

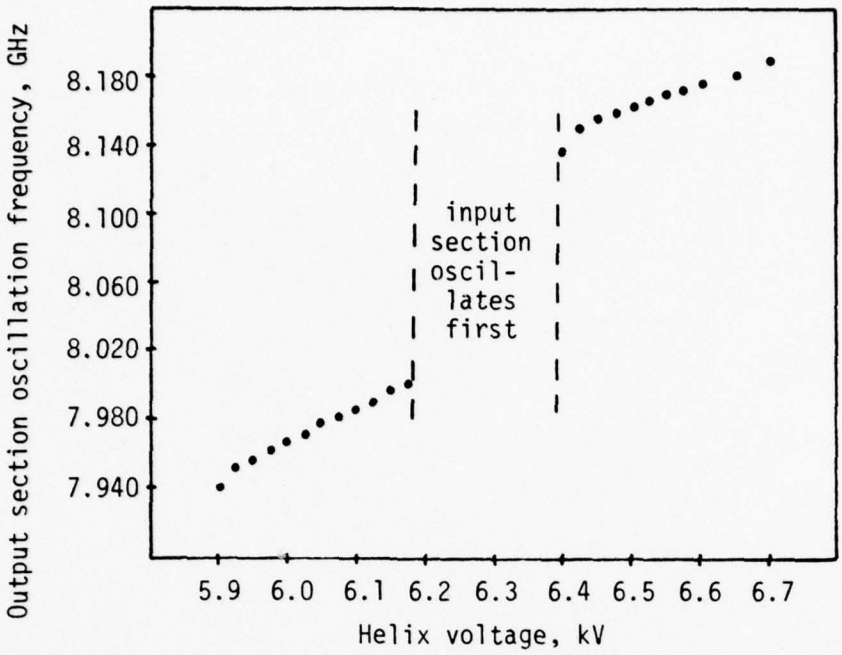

Figure 8a. Oscillation frequency vs. helix voltage for the output section of the WJ-3633-5. Between 6200 and 6400 volts, the input section oscillated at a lower start current than the output section, preventing measurement on the latter.

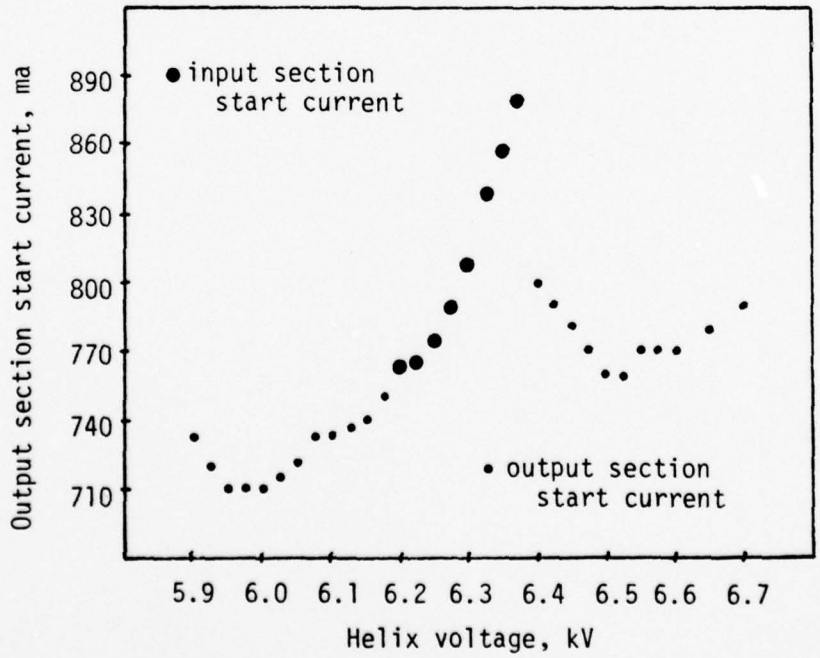

Figure 8b. Output section start current vs. helix voltage corresponding to the measurements in figure 8a. Input start current is indicated between 6200 and 6400 volts as a lower bound on output start current.

For helix voltages between 6200 and 6400 volts, the input helix section oscillated before the output helix start current was reached, preventing measurements on the output section.* In this voltage range, the start current for input helix oscillation is indicated as a lower bound for output helix start current. When interpreted as described in the previous paragraph, these figures imply the presence of a stop band on the output helix section near 8.06 GHz with a width of approximately 140 MHz. (Analagous data for the input helix section, which appears in the appendix, displays the typical appearance of a stop band, and should be compared to figures 8a and 8b.)

Measurements of the reflection coefficient looking into the output of the WJ-3633-5 support the conclusions based on output helix oscillation frequencies and start currents. This reflection coefficient indicates the quality of the match between the helix and coaxial output transmission line, but the effect of an offset support rod, as discussed previously, should increase the reflection coefficient in the vicinity of the stop band. Measurement of the magnitude of the reflection coefficient vs. frequency for the output section of the WJ-3633-5 appears in figure 9. The large peak implies the presence of a stop band centered at 8.07 GHz with width of approximately 180 MHz, corroborating previous measurements.

In addition to their consistency with one another, the various

*Output section oscillations appear only at the TWT output; input section oscillations appear at the TWT input, and are carried onto the output section by the electron beam, as well. Hence, output section oscillations cannot be investigated if the associated start current exceeds the input section start current.

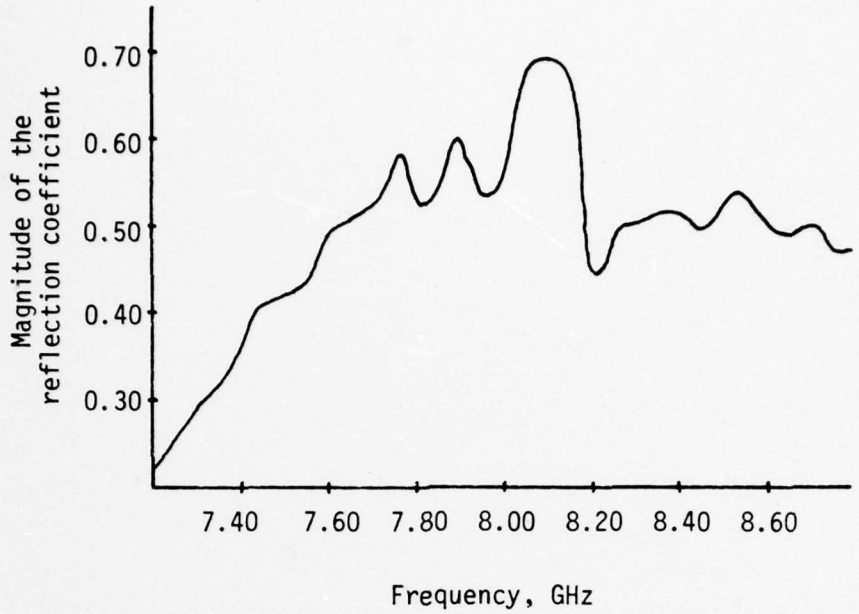

Figure 9. Magnitude of the reflection coefficient vs. frequency looking in the output of the WJ-3633-5.

characteristics of the stop band determined from these three sets of measurements compare well with the predictions of the theoretical model. An output helix section constructed on the same apparatus as (and, therefore, expected to be identical to) the one in the WJ-3633-5 under investigation contained a helix support rod misaligned by 10^0 (0.2 radians). For a reasonable value of $|\rho_0|$ (1/40), equation 8 predicts a fractional stop band width of 1%. At a crossover frequency of 8.0 GHz, this corresponds to a stop band width of 80 MHz, in reasonable agreement with measurements, considering the simplicity of the model. (Recall that the model considers only misaligned support rods, and neglects other effects which contribute to the formation of this stop band). Consequently, the presence and dimensions of a stop band at the crossover frequency on the output helix of this WJ-3633-5 are established with good certainty.

III.A.2 GENERAL APPEARANCE OF POWER SUCK-OUT

As mentioned previously, power suck-out occurs commonly in high power single helix dual mode amplifiers. Preliminary measurements indicated the presence of the phenomenon in the WJ-3633-5 near one half the crossover frequency (8.00 GHz), in accordance with results preceding this report (item c, page 3). Section III.A.2 discusses the general features of power suck-out as it appeared in this TWT. Measurements were performed to investigate the dependence of power suck-out on cathode current, helix voltage, and input power. This section concludes with a brief look at the harmonic characteristics of this tube which relate to power suck-out.

Dependence on cathode current. Initial observations indicated that an increase in cathode current near the start oscillation current rapidly enhances power suck-out. Accordingly, most measurements on this WJ-3633-5 were performed at a beam current only slightly lower than the current at which oscillation occurs without rf drive (the maximum current for useful operation) so that the appearance of the power holes is most pronounced. A sufficient reduction in beam current diminishes the depth of the power holes so that they no longer present a limitation to tube operation. In this sense, power suck-out places an upper limit on the useful beam current and hence the pulse-up power available in a dual mode tube.

Dependence on helix voltage. Each of the figures 10a-10k displays the power transfer curve of the tube (fundamental output power vs. frequency) at various helix voltages. The cathode

current of 0.700 amps and input power (held constant with frequency) 10 db below saturation drive* remain constant in this series of measurements. At these values, the power holes are most easily observable for two reasons. First, the maximum depth of the power holes for a constant cathode current and helix voltage occurs with input power 10 db below saturation drive. Second, any increase in cathode current would cause the tube to oscillate at one or more of the helix voltages of interest, so that 0.700 amps represents the maximum current useful over the full voltage range.

The two distinct power holes (indicated by arrows), characteristic of power suck-out, appear over only a limited range of helix voltages. The depth and frequency of both power holes depend on voltage as follows. Each has a helix voltage of maximum depth, around 6000 volts for the lower frequency power hole (figure 10d), and 6600 volts for the upper frequency power hole (figure 10j). Each decreases in depth as voltage is adjusted away from the voltage where it predominates. Furthermore, the frequency of each power hole increases with voltage, as summarized in figure 10l. It should be emphasized that the two frequencies tune continuously with voltage, with no discrete jumps observed.

An additional comment is in order here. The depth of the power holes listed in figure captions was measured with an accurate thermoelectric power meter. But the fundamental output power displayed in figures 10a-10k was measured with a crystal detector.

*Throughout the report, the input power is measured relative to the value required for saturation, referred to as saturation drive.

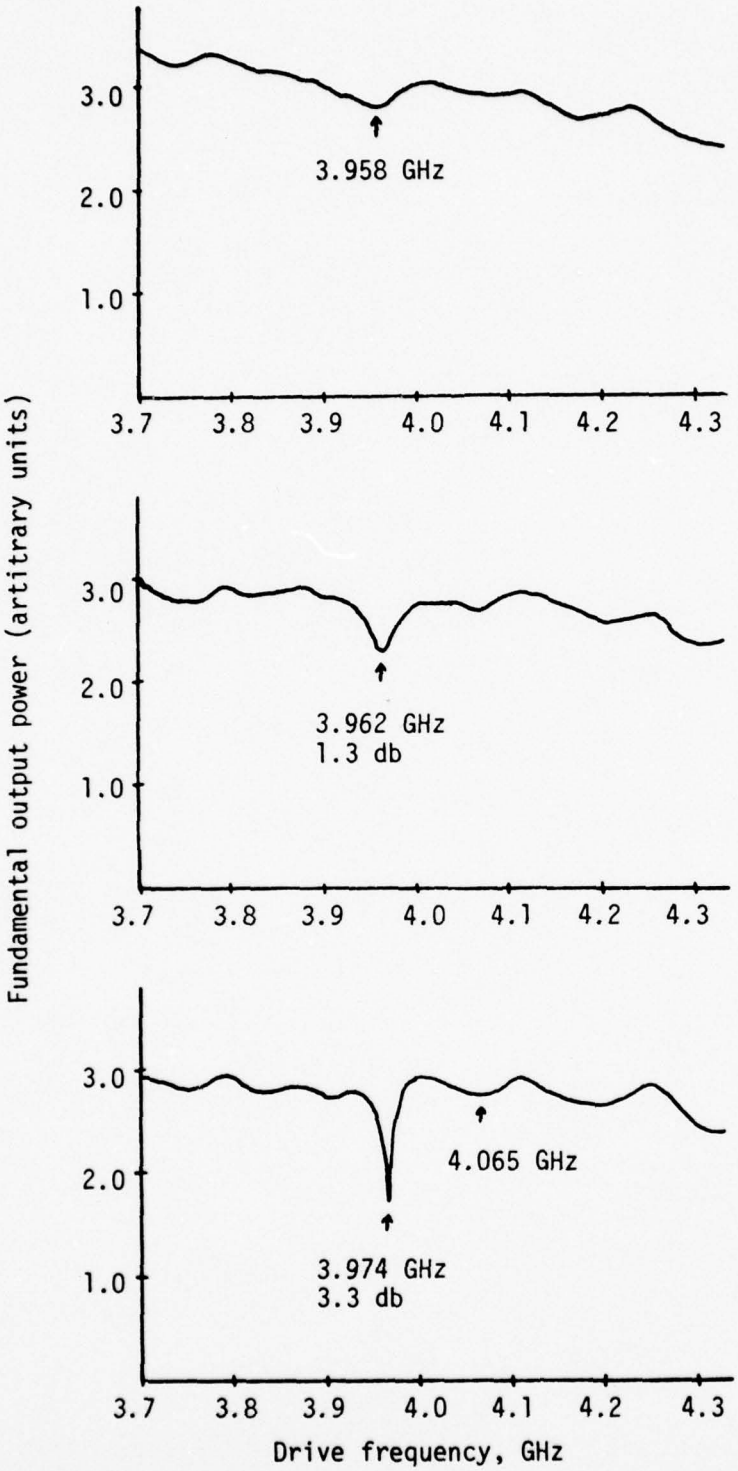

Figure 10a.
Helix voltage
=5700 volts.

Figure 10b.
Helix voltage
=5800 volts.

Figure 10c.
Helix voltage
=5900 volts.

Figures 10a, 10b, 10c. Fundamental output power vs drive frequency for various helix voltages. Cathode current is 0.700 amps. Input power is 10 db below saturation drive. Power holes are indicated by arrows along with their frequency and depth.

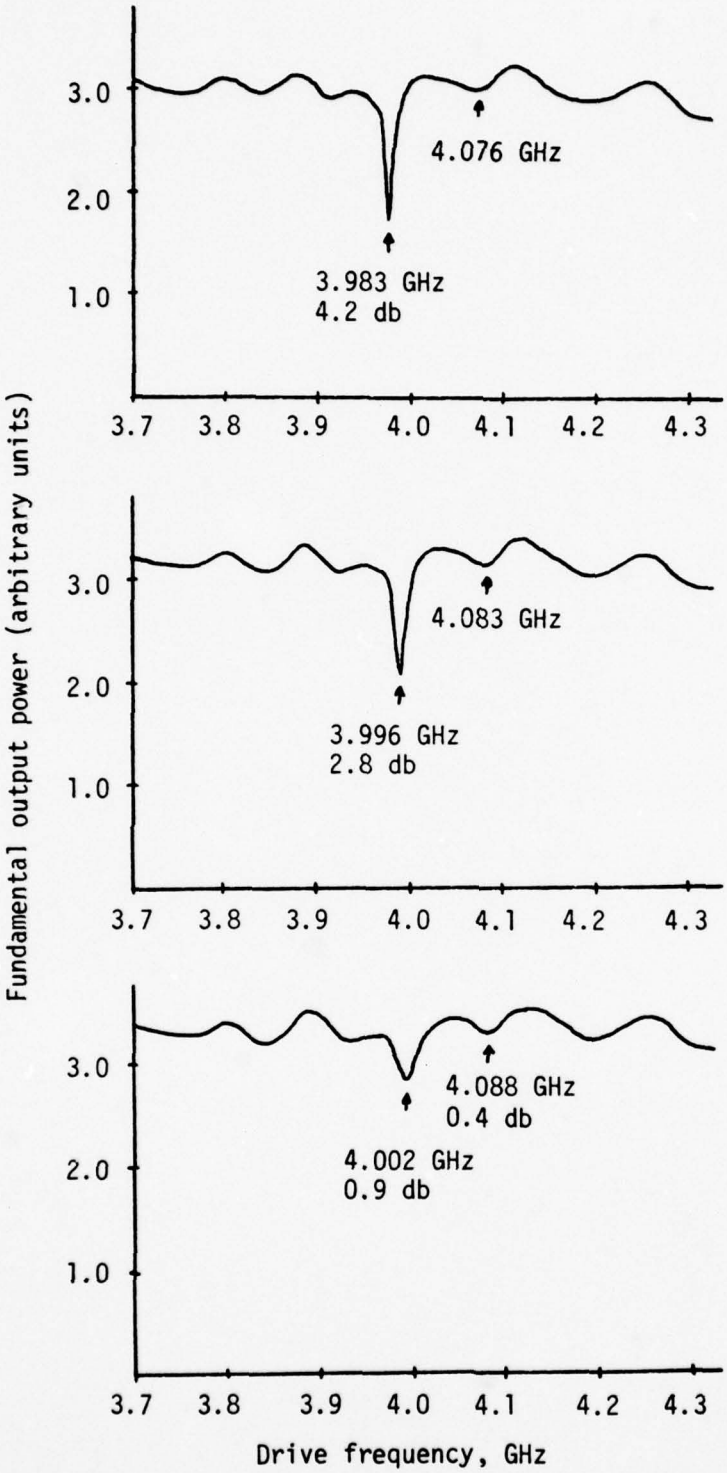

Figure 10d.
Helix voltage
=6000 volts.

Figure 10e.
Helix voltage
=6100 volts.

Figure 10f.
Helix voltage
=6200 volts.

Figures 10d, 10e, 10f. Fundamental output power vs. drive frequency for various helix voltages. Cathode current is 0.700 amps. Input power is 10db below saturation drive. Power holes are indicated by arrows along with their frequency and depth.

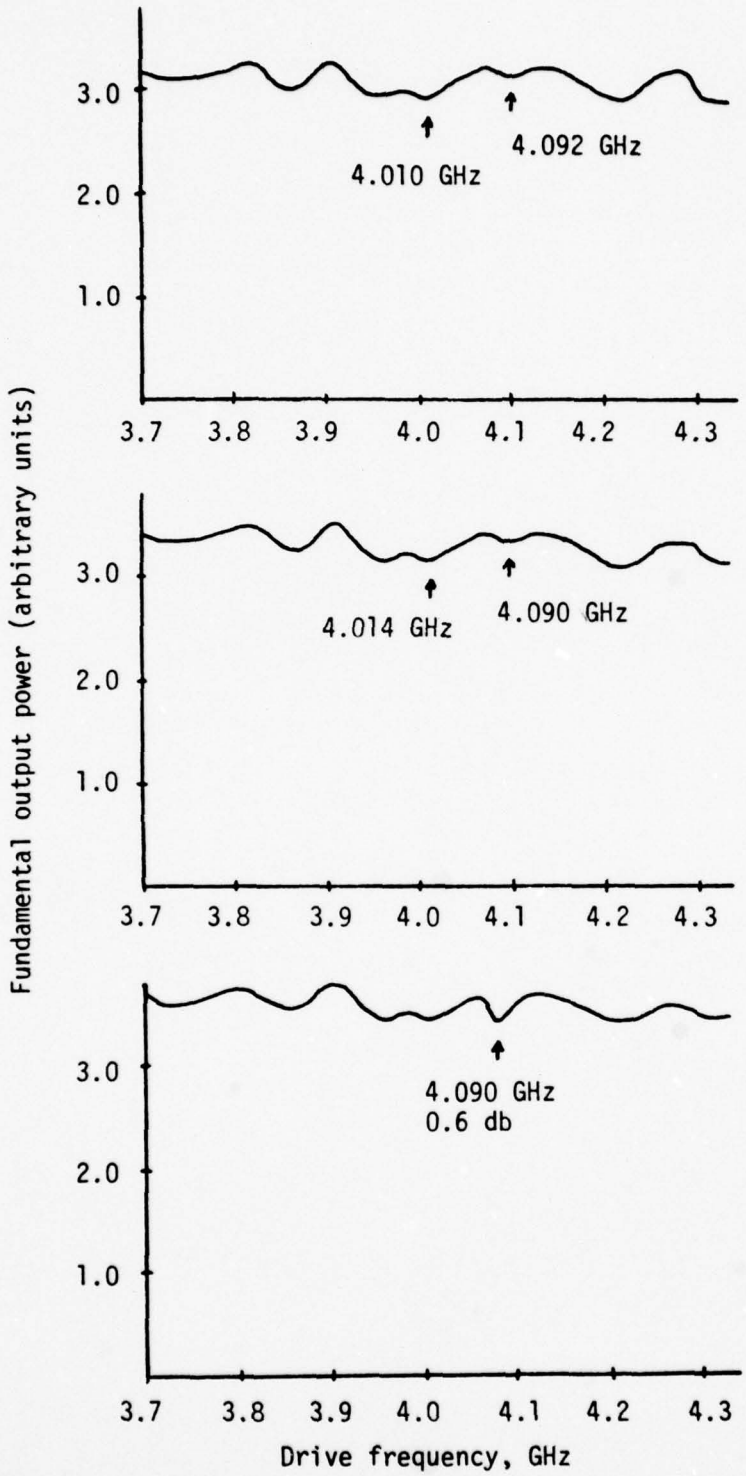

Figure 10g.
Helix voltage
=6300 volts.

Figure 10h.
Helix voltage
=6400 volts.

Figure 10i.
Helix voltage
=6500 volts.

Figures 10g, 10h, 10i. Fundamental output power vs. drive frequency for various helix voltages. Cathode current is 0.700 amps. Input power is 10 db below saturation drive. Power holes are indicated by arrows along with their frequency and depth.

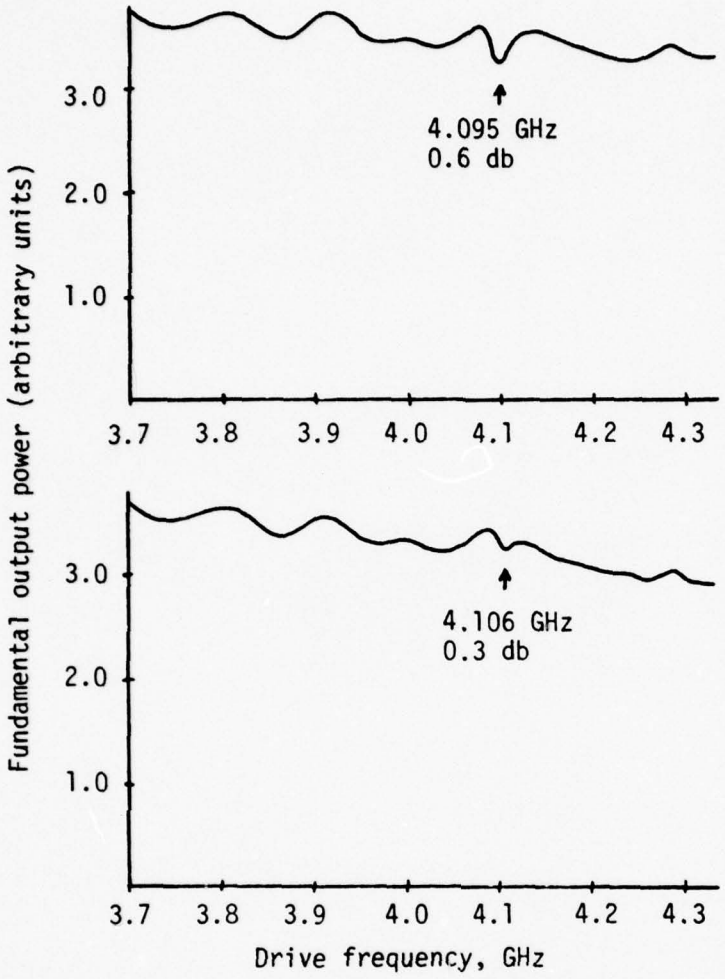

Figure 10j.
Helix voltage
=6600 volts.

Figure 10k.
Helix voltage
=6700 volts.

Figures 10j, 10k. Fundamental output power vs. drive frequency for various helix voltages. Cathode current is 0.700 amps. Input power is 10 db below saturation drive. Power holes are indicated by arrows along with their frequency and depth.

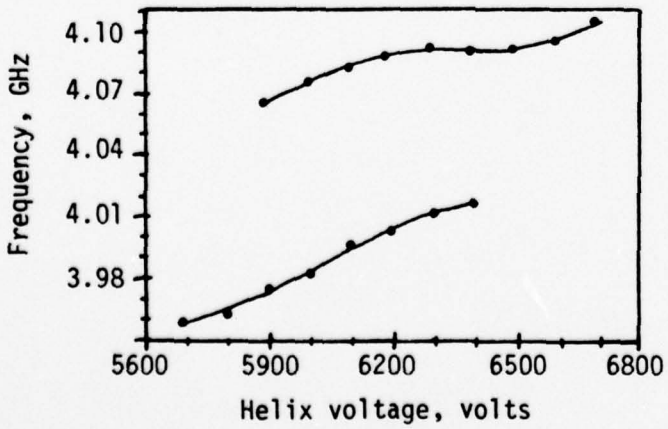

Figure 10l. Frequency of power holes vs. helix voltage.

Since the latter device proved to be slightly nonlinear, the ordinates, though nearly linear in gain, are labeled only with an arbitrary scale for purposes of comparison between figures. The objective in these figures is to show the nature of the phenomenon and to begin to characterize it from a general starting point. The relatively fast response time of a crystal detector allows measurement of output power while input power is swept in frequency. This greatly expedites the measurement of data displayed in these figures. The same comments apply to figures 11a-11g and 12a-12f, which are presented later. More accurate evaluation of gain and output power appears in subsequent sections.

A question may arise regarding figures such as 10h and the interpretation of slight gain variations as power suck-out. In cases such as this, an increase in the beam current with simultaneous increase of drive level to eliminate oscillations sufficiently enhanced the effect to allow its identification at the frequencies indicated. Furthermore, observation of the behavior of the power hole as helix voltage was varied allowed unambiguous identification of power suck-out, even when the effect was minimal.

Dependence on input power. Next, the behavior of power suck-out as a function of input power is considered. Measurements of fundamental output power, P, and helix interception current, i, vs. frequency, at various drive levels, appear in figures 11a-11g and 12a-12f. Helix voltage and cathode current are held constant within each set of figures. The helix voltage where the lower frequency power hole predominates, and helix voltage where the upper frequency power hole predominates determine the choice of

voltages in figures 11a-11g and figures 12a-12f, respectively. The cathode current chosen in each case is only slightly less than the start oscillation current at that voltage to enhance the appearance of the power suck-out. Within each figure, input power is constant over the frequency range of interest. In these figures, note that fundamental output power is measured from the bottom of the figure and calibrated on the left vertical scale, while helix interception current is measured from the top of the figure and calibrated on the right vertical scale.

The following features of figures 11a-11g describing the lower frequency power hole deserve comment. With the tube overdriven (figure 11a), the power hole is shallow. As drive is reduced, the depth of the power hole increases to its maximum value with input power 10 db below saturation drive. As the power hole grows, a decrease in helix current appears at the same frequency. It occurs most visibly where the power hole is deepest, in figure 11d. As drive is reduced further, the dip in helix current becomes a peak, and the power hole shifts to a higher frequency and becomes narrower. Finally, the appearance of the very narrow abrupt dip in fundamental output power and the corresponding peak in helix interception current in figure 11g suggest the presence of an oscillation. Both the effects apparent in figure 11g disappear at lower drive levels.

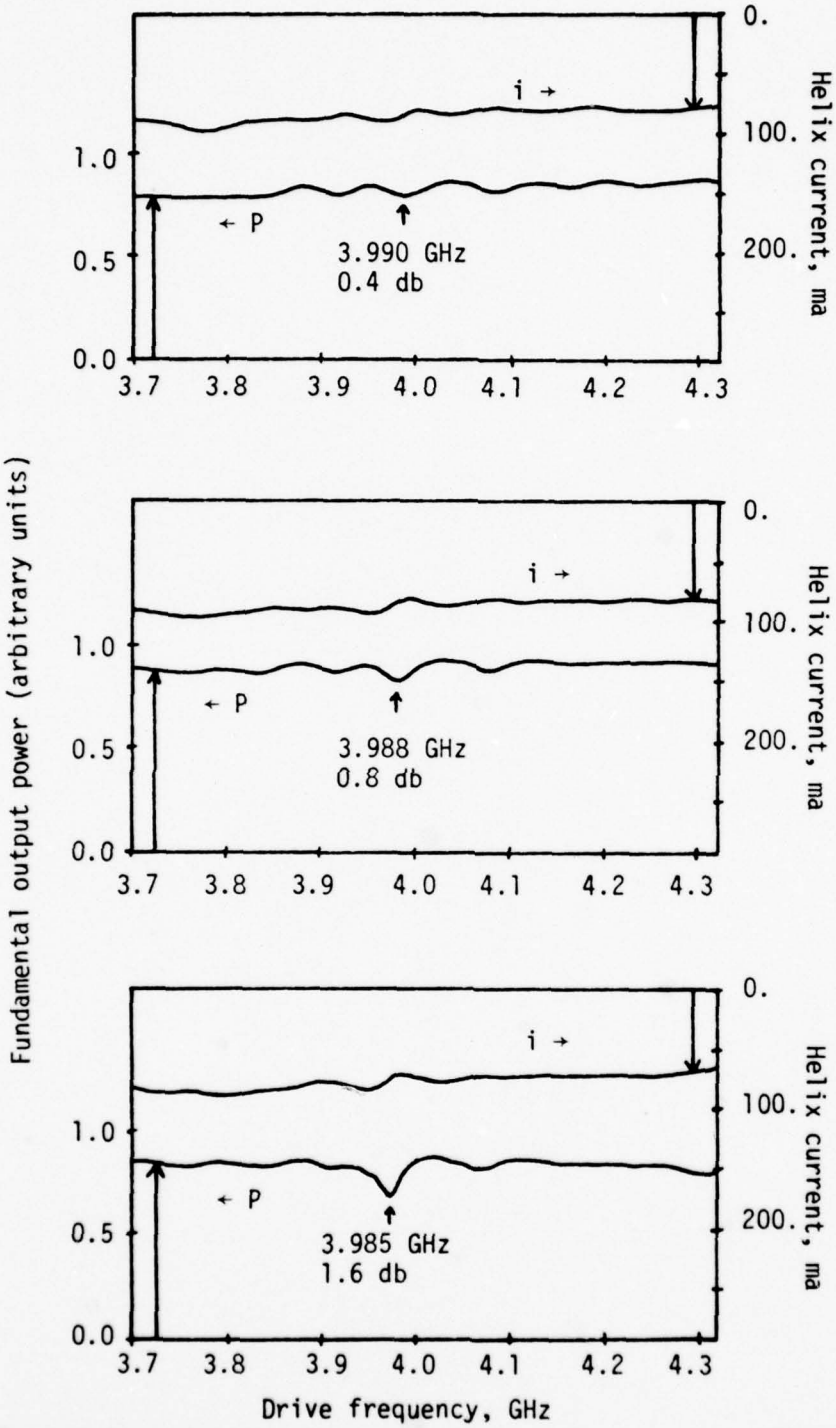

Figure 11a. Input power 3 db above saturation drive.

Figure 11b. Input power at saturation drive.

Figure 11c. Input power 5 db below saturation drive.

Figures 11a, 11b, 11c. Fundamental output power, P, and helix interception current, i, vs. drive frequency for various levels of input power. Cathode current is 0.690 amps. Helix voltage is 6000 volts. Power holes are indicated by arrows.

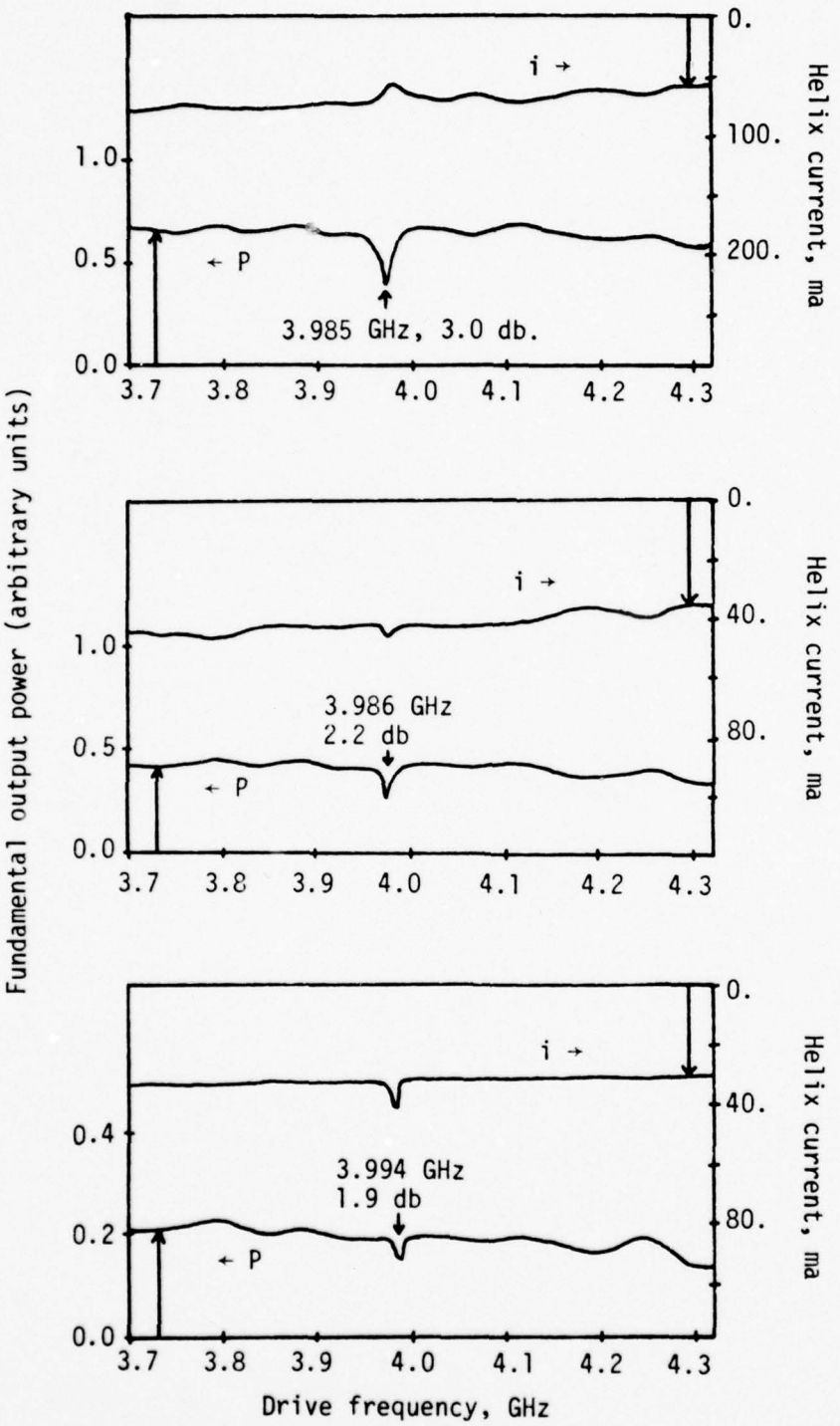

Figure 11d. Input power 10 db below saturation drive.

Figure 11e. Input power 15 db below saturation drive.

Figure 11f. Input power 20 db below saturation drive.

Figures 11d, 11e, 11f. Fundamental output power, P, and helix interception current, i, vs. drive frequency for various levels of input power. Cathode current is 0.690 amps. Helix voltage is 6000 volts. Power holes are indicated by arrows.

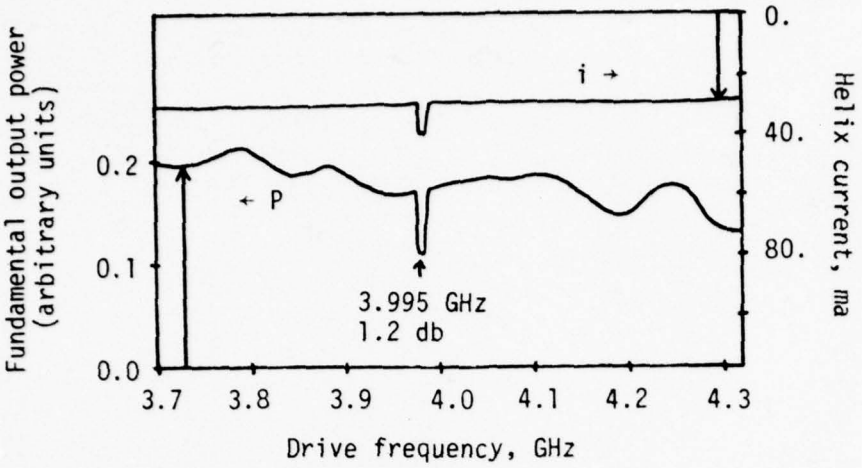

Figure 11g.
Input power 25 db
below saturation
drive.

Figure 11g. Fundamental output power, P, and helix interception current, i, vs. drive frequency. Cathode current is 0.690 amps. Helix voltage is 6000 volts. Power hole is indicated by arrow.

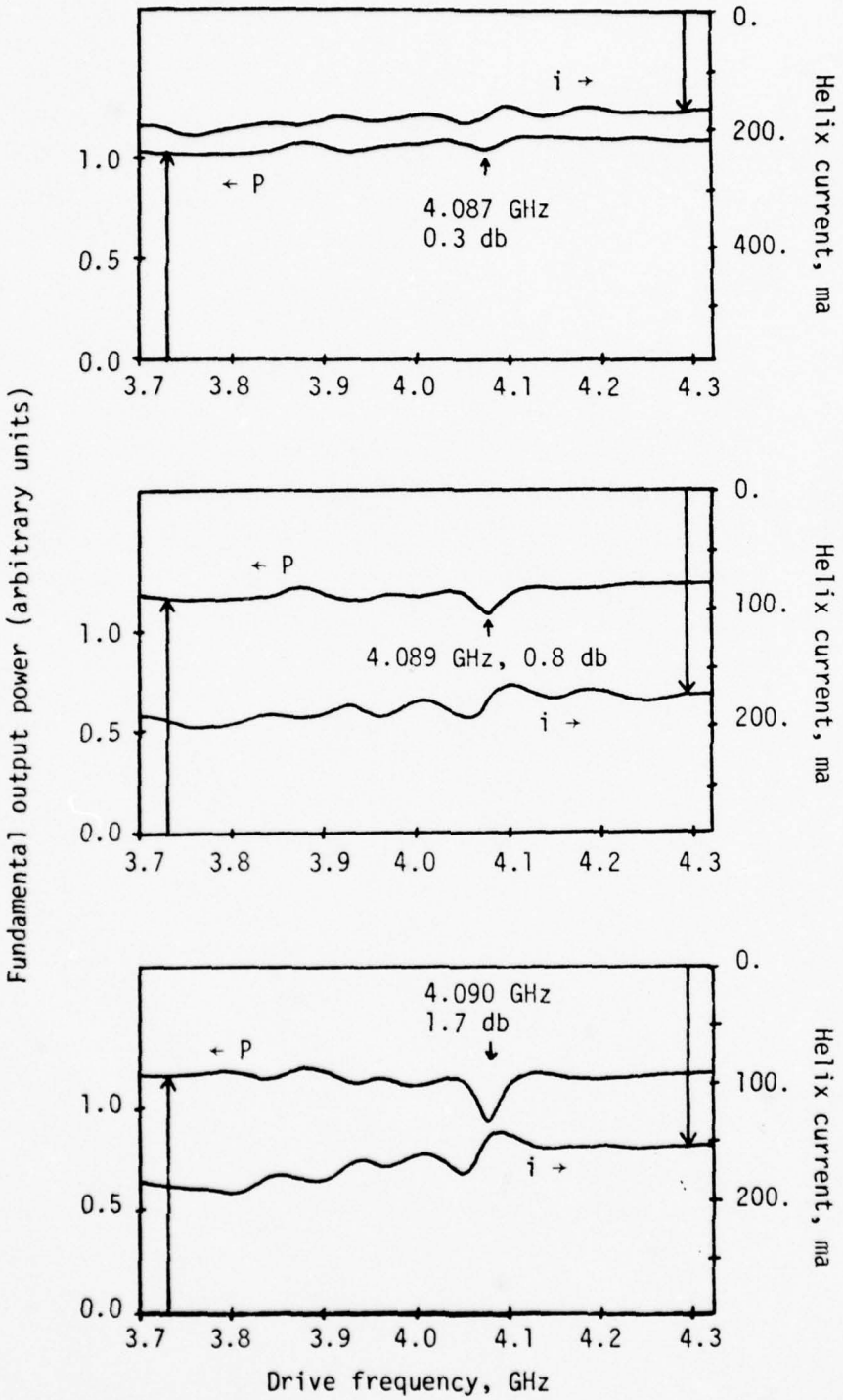

Figure 12a. Input power 3 db above saturation drive.

Figure 12b. Input power at saturation drive.

Figure 12c. Input power 5 db below saturation drive.

Figures 12a, 12b, 12c. Fundamental output power, P, and helix interception current, i, vs. drive frequency for various levels of input power. Cathode current is 0.750 amps. Helix voltage is 6600 volts. Power holes are indicated by arrows.

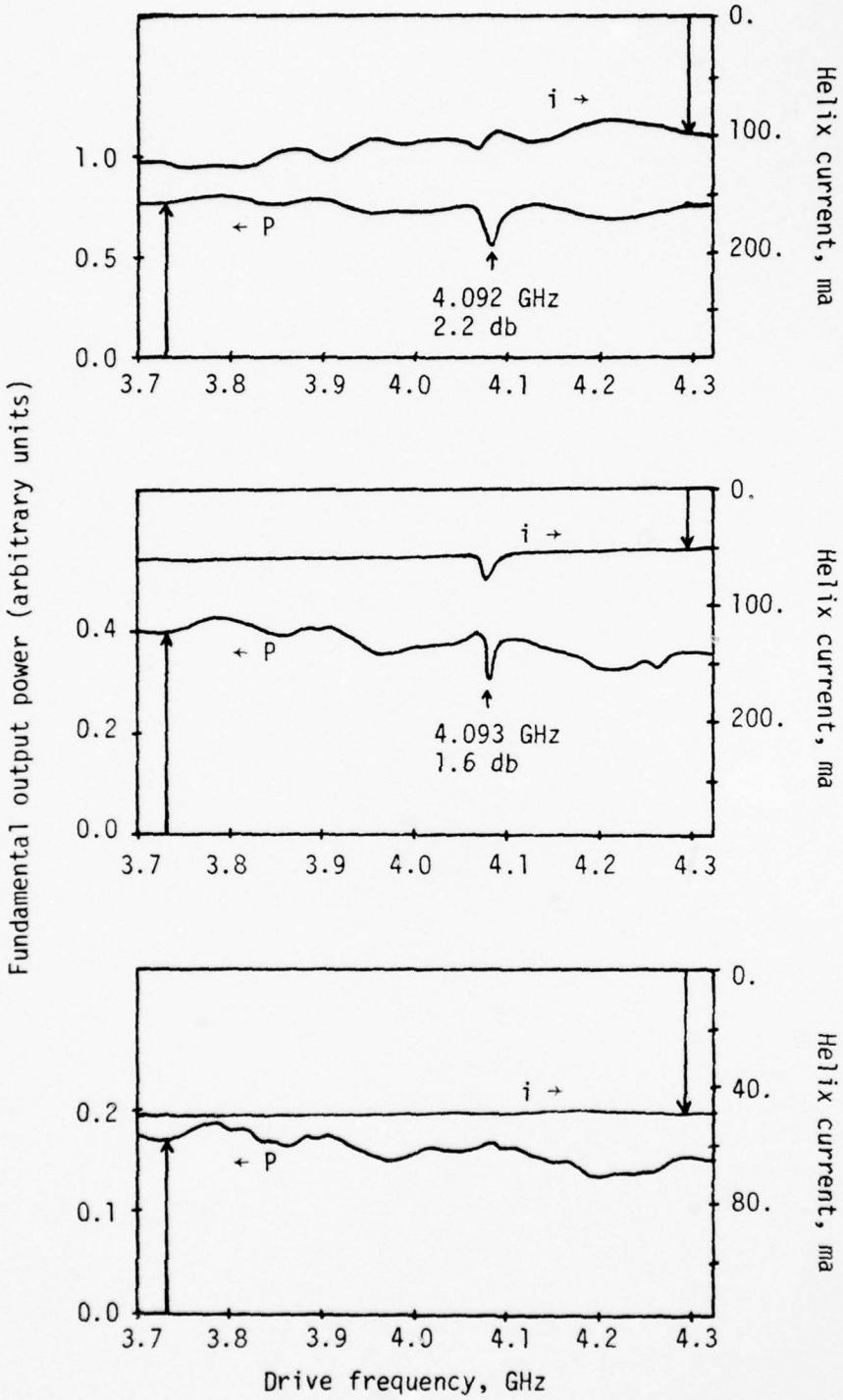

Figure 12d. Input power 10 db below saturation drive.

Figure 12e. Input power 15 db below saturation drive.

Figure 12f. Input power 20 db below saturation drive.

Figures 12d, 12e, 12f. Fundamental output power, P, and helix interception current, i, vs. drive frequency for various levels of input power. Cathode current os 0.750 amps. Helix voltage is 6600 volts. Power holes are indicated by arrows.

The same comments apply to figures 12a-12f which describe the upper frequency power hole. Only slight variations of fundamental output power and helix interception current appear when the tube is overdriven. The dips in fundamental output power and helix current increase to maximum magnitude in figure 12c, and for lower drive levels the narrow dip in output power and corresponding peak in helix current again suggest a tube oscillation (figure 12e). At low enough input power, the phenomenon is absent (figure 12f).

Note also the change in frequency of power suck-out as drive level changes. This occurs at both helix voltages, 6000 volts (figures 11a-11g) and 6600 volts (figures 12a-12f). The apparent oscillation which occurs at lower input power levels (15 to 20 db below saturation drive) may account for part of this change. More definite comment on this feature and on the relationship between power suck-out and helix interception current at various drive levels and beam currents requires further investigation.

Harmonic output power. The possibility that the tube oscillates at discrete frequencies under conditions such as those in figure 11g or 12e creates interest in the harmonic power output. With the tube driven at the fundamental, a pair of crystal detectors simultaneously measure fundamental and second harmonic output power vs. frequency. Figure 13 displays the results under the following conditions: fundamental output power corresponds to input power 8 db below saturation drive, helix voltage is 6000 volts, and cathode current is 0.700 amps. Fundamental output power is roughly 10 db above second harmonic, but the behavior of crystal detectors prevents accurate comparisons here. More precise

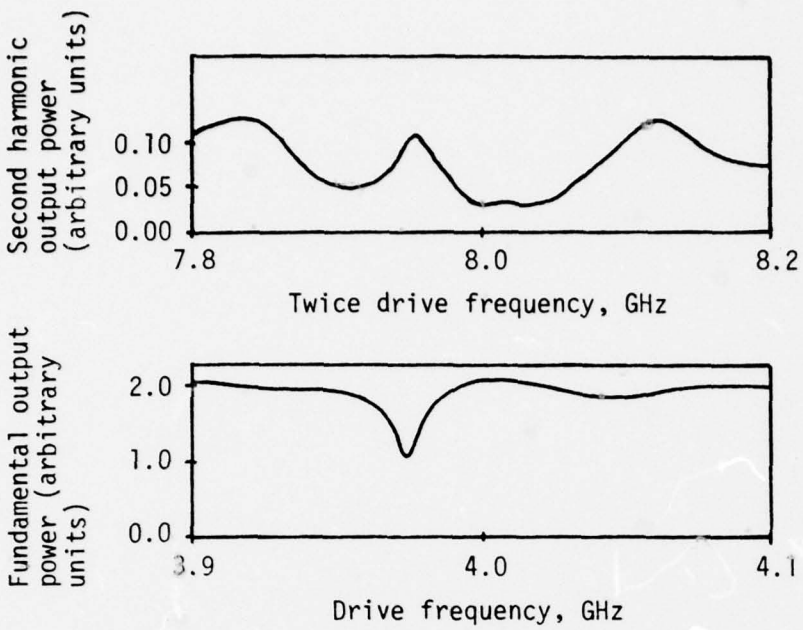

Figure 13. Fundamental and second harmonic output power vs. frequency when driving at the fundamental. Helix voltage is 6000 volts. Cathode current is 0.700 amps. Fundamental output power corresponds to input power 8 db below saturation drive. Note that the second harmonic output power is roughly 10 db below fundamental output power.

measurements are described in ensuing pages. Notice the presence of the familiar dip in output power at the fundamental with the peak in second harmonic power at precisely twice this frequency. The magnitude of the peak in second harmonic output power is not sufficient to account for all the power "missing" at the fundamental. Neither can the presence of the second harmonic peak alone explain the power hole at fundamental, since other peaks in second harmonic output power appear in figure 13 with no corresponding power hole in the fundamental.

All data presented in section III.A.2 involves swept frequency measurements. Crystal detectors permit these fast, convenient measurements, which nevertheless effectively describe the general behavior of power suck-out. More accurate determination of such

quantities as gain or power output with thermoelectric power meters requires continuous tube operation at single frequencies to accommodate the slower response time. In order to more closely observe the detailed behavior of power suck-out, this latter type of measurement was performed.

III.A.3 QUANTITATIVE BEHAVIOR OF POWER SUCK-OUT

Section III.A.2 provides a general overview of the behavior of power suck-out. Sections III.A.3 through III.A.5 proceed from those observations to investigate the details of the phenomenon in a more quantitative manner. Specifically, section III.A.3 concentrates on TWT bwhavior when driving at frequencies in the vicinity of the two power holes which characterize power suck-out.

The lower frequency power hole. Figures 14a, 14b, and 14c display results of measuring fundamental output power, helix current, and second harmonic output power, respectively, vs. input power driving at three particular frequencies of interest. These frequencies lie in the vicinity of the lower frequency power hole (see figure 10d), with the selection of helix voltage (6000 volts) and cathode current (0.670 amps) corresponding to where this power hole is substantial. In each of these three figures, the solid line represents data taken with the tube driven at 3.950 GHz, adjacent to but unaffected by the power hole. The drive frequency of the dashed curves is 3.985 GHz, where maximum power suck-out occurs with input power 10 db below saturation drive, as in figure 11d. The dotted curve corresponds to input at 3.994 GHz, where the apparent oscillation occurs with input power 25 db below saturation drive, as in figure 11g. Note in figure 11d that the width of the lower frequency power hole

is approximately 25 MHz. Also, the dependence of power hole frequency on drive level indicated in figures 11a-11d involves changes of only a few megahertz. So within 15 db of saturation, the data at 3.985 GHz (dashed curves) should represent tube behavior in the power hole to good accuracy.

In figures 14a, 14b, and 14c the solid curves display the features of conventional tube operation. The gain at the fundamental is constant until near saturation where the fundamental output power levels off and decreases in overdrive (figure 14a). Helix current steadily increases with input power until near saturation where its functional behavior becomes complex (figure 14b). Second harmonic output power increases steadily with input power, reaching its largest value with the tube slightly overdriven (figure 14c).

The dashed curves display characteristics of power suck-out as deviations from normal tube operation (the solid curves). As expected, the phenomenon is absent at low input power levels. A deficiency in both fundamental output power and helix current begins to appear with input power 15 db below saturation drive (figures 14a and 14b). The dips in fundamental output power and helix current grow to their largest magnitudes near 10 db below saturation drive. At increasing input power levels, the discrepancies decrease and disappear with the tube overdriven. At all power levels, the second harmonic output power with input at the frequency of the power hole is greater than with input at an adjacent frequency (dashed and solid curves, respectively, figure 14c), as is expected from figure 13.

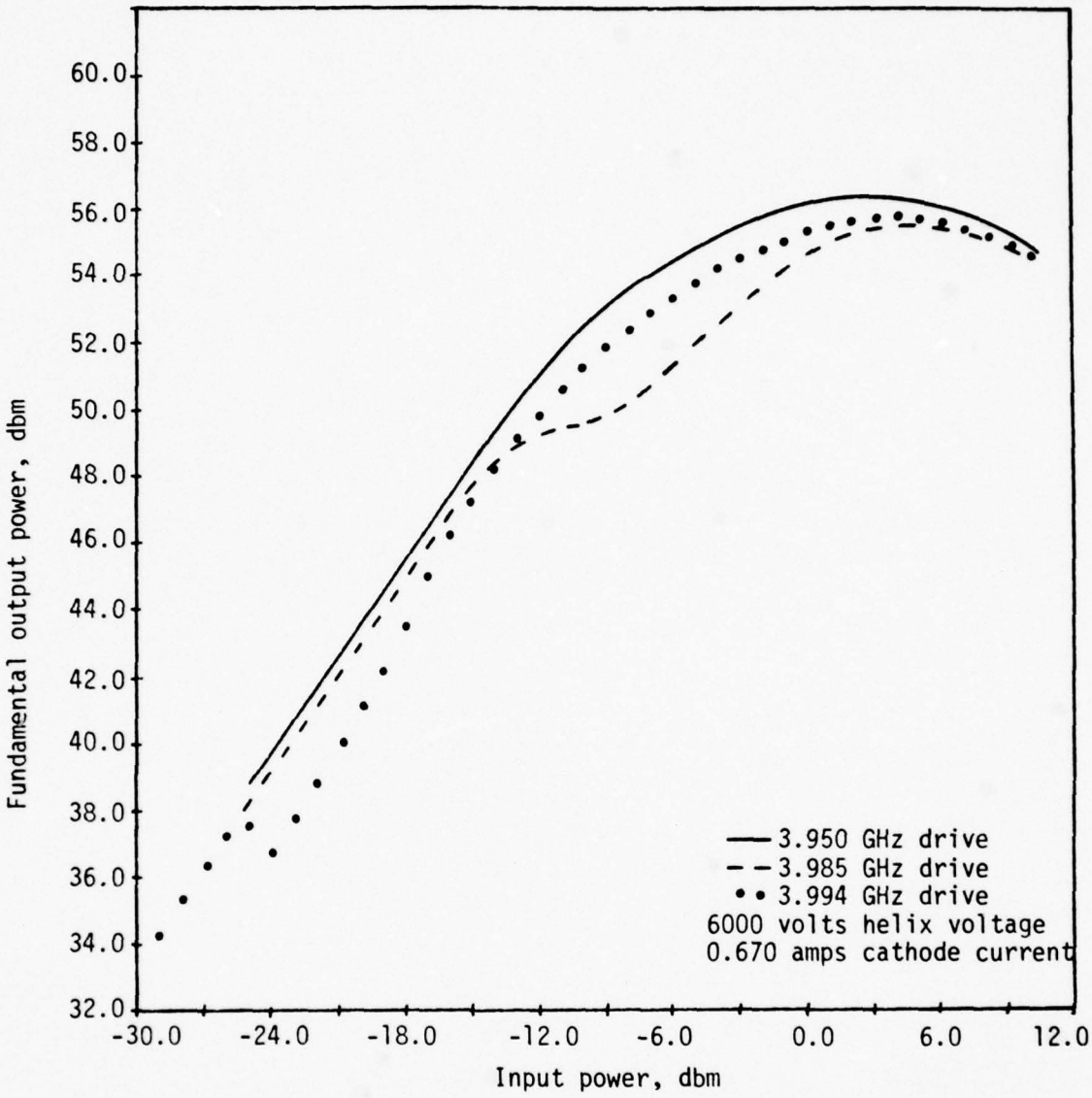

Figure 14a. Fundamental output power vs. input power (driving at the fundamental) at three frequencies of interest. Solid line corresponds to input at 3.950 GHz, adjacent to but unaffected by the power hole. Dashed line corresponds to input at 3.985 GHz, the center of the power hole with input 10 db below saturation drive. Dotted line corresponds to input at 3.994 GHz, the drive frequency where oscillation occurs with input 25 db below saturation drive.

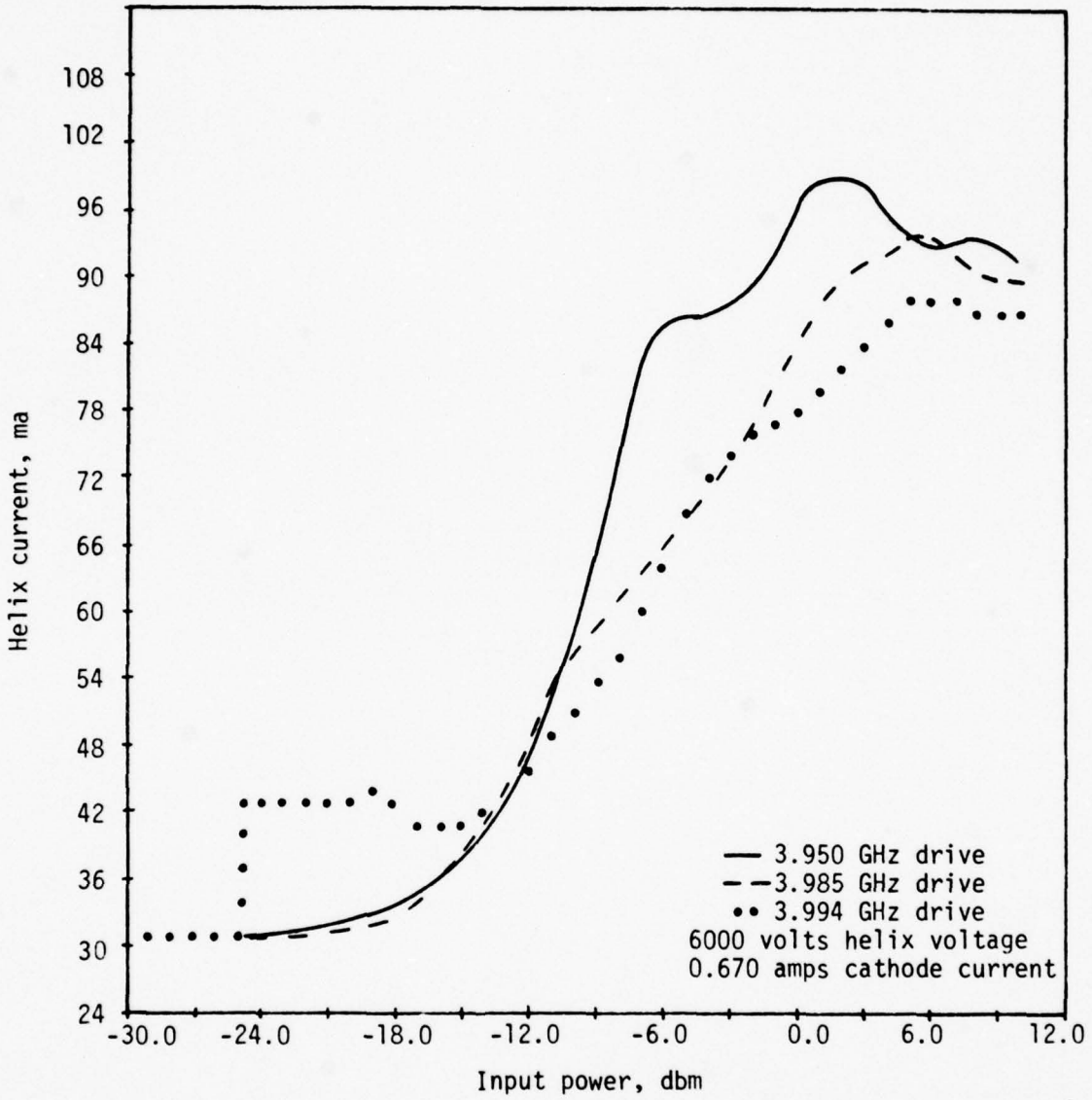

Figure 14b. Helix current vs. input power (driving at the fundamental) at three frequencies of interest. Solid line corresponds to input at 3.950 GHz, adjacent to but unaffected by the power hole. Dashed line corresponds to input at 3.985 GHz, the center of the power hole with input 10 db below saturation drive. Dotted line corresponds to input at 3.994 GHz, the drive frequency where oscillation occurs with input power near 25 db below saturation drive.

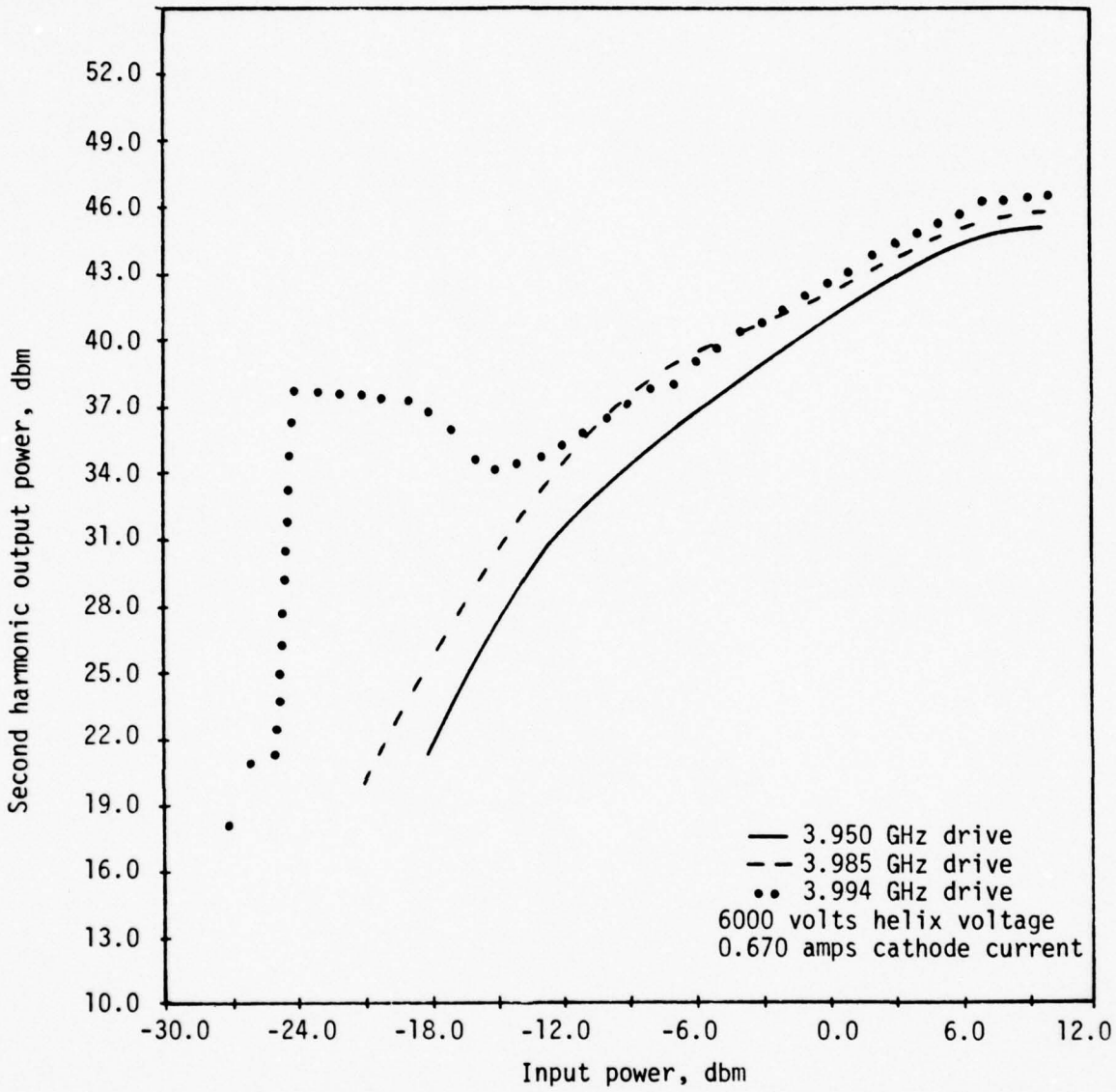

Figure 14c. Second harmonic output power vs. input power (driving at the fundamental) at three frequencies of interest. Solid line corresponds to input at 3.950 GHz, adjacent to but unaffected by the power hole. Dashed line corresponds to input at 3.985 GHz, the center of the power hole with input 10 db below saturation drive. Dotted line corresponds to input at 3.994 GHz, the drive frequency where oscillation occurs with input 25 db below saturation drive. In the region where the dotted curve levels off (between -16.0 dbm and -24.0 dbm input power) the frequency of "second harmonic" output is 7.975 GHz. On the remainder of this curve and on the entire other two curves, second harmonic output is at exactly twice the drive frequency.

The dotted curves illustrate modifications of the transfer characteristics caused by the oscillation which occurs when the tube is driven at 3.994 GHz. It predominates at input power levels 25 db below saturation drive. In this region the helix current and "second harmonic" output power are independent of drive level. The tube appears to be operating as a "locked oscillator". Reduction of drive level below a threshold value of -24 dbm results in abrupt changes in fundamental output power, "second harmonic" output power, and helix current to values consistent with normal tube operation (solid curves). "Second harmonic" output power is referred to with quotes because in the region of oscillation the frequency of this output power is not precisely twice the drive frequency. At all other drive levels on the dotted curve, and at all portions of the other two curves of figure 14c the second harmonic is exactly twice the drive frequency. So there indeed appears to be a drive-associated oscillation in the vicinity of the power hole for tube operation at these values of helix voltage and cathode current. When driving the tube at 3.994 GHz (2f = 7.988 GHz), an oscillation at 7.975 GHz occurs under very specific conditions.

Measurements analagous to those in figure 14 were performed while operating the tube at the same helix voltage (6000 volts), but with a lower cathode current (0.630 amps). Under these conditions no oscillation of the type described in the preceding paragraph appeared. Figures 15a, 15b, and 15c display fundamental output power, helix current, and second harmonic output power, respectively, vs. input power (driving at the fundamental) at two frequencies of interest. As before, the solid curves display measurements with

input at 3.950 GHz, adjacent to and unaffected by power suck-out. The drive frequency of the dashed curves is 3.986 GHz, where maximum power suck-out occurs.

Once again, the solid curves exhibit normal tube operation, while the dashed curves display tube behavior with input at the frequency of the power hole. At low input power levels, the power hole is absent. The fundamental output power and helix current when driving at 3.986 GHz begin to deviate from expected values (the solid curves) with input power 12 db below saturation drive. The deficiencies in these two quantities associated with the power hole reach their largest value with input 8 db below saturation drive, and then decrease with increasing input power eventually disappearing in overdrive (figures 15a and 15b). Second harmonic output power is somewhat greater when the tube is driven at the frequency of the power hole than at an adjacent frequency (figure 15c).

The measurements performed at a beam current of 0.670 amps and displayed in figure 14 appear almost identical to those performed at a beam current of 0.630 amps, summarized in figure 15. Two exceptions are noted. First, the deficiencies in fundamental output power and helix current associated with the power hole are more pronounced at the higher beam current, as is expected from previous observations. Second, and more important, the drive-associated oscillation which occurs under specific conditions at the higher beam current is absent at the lower current. So the drive-associated oscillation and power suck-out phenomena are distinct effects, though explanations of their occurance may be closely related.

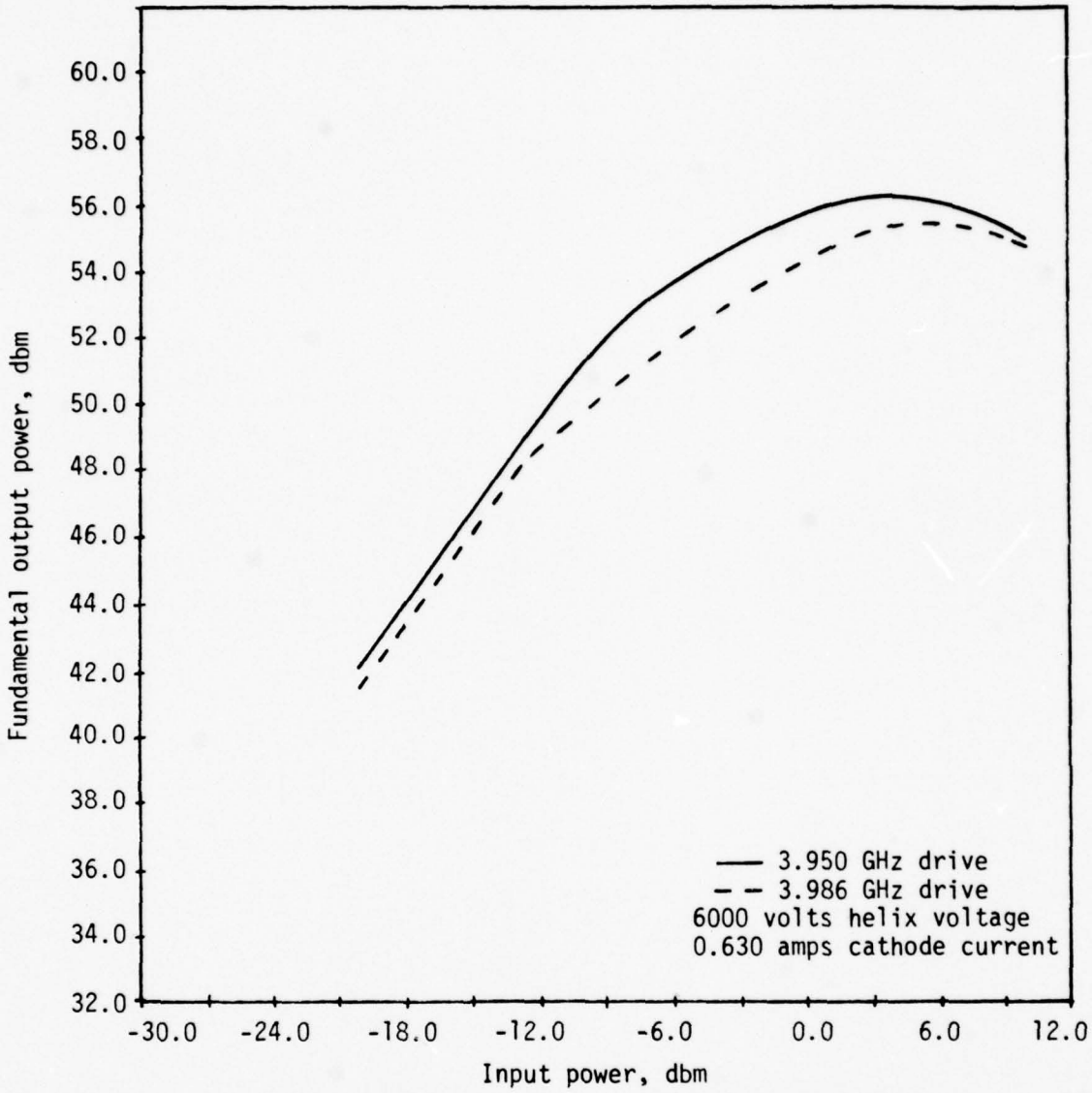

Figure 15a. Fundamental output power vs. input power (driving at the fundamental) at two frequencies of interest. Solid line corresponds to input at 3.950 GHz, adjacent to but unaffected by the power hole. Dashed line corresponds to input at 3.986 GHz, the center of the power hole.

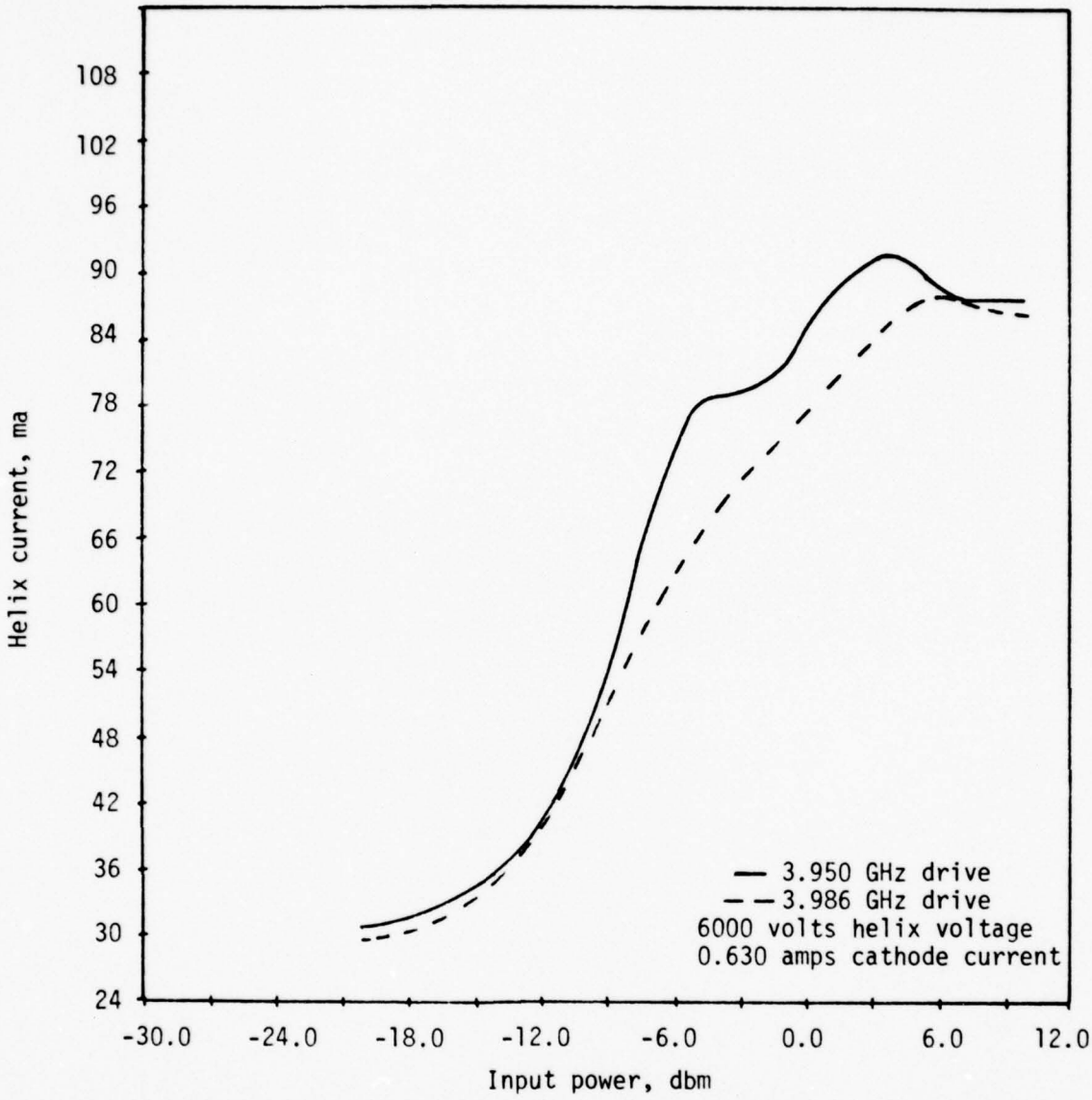

Figure 15b. Helix current vs. input power (driving at the fundamental) at two frequencies of interest. Solid line corresponds to input at 3.950 GHz, adjacent to but unaffected by the power hole. Dashed line corresponds to input at 3.986 GHz, the center of the power hole.

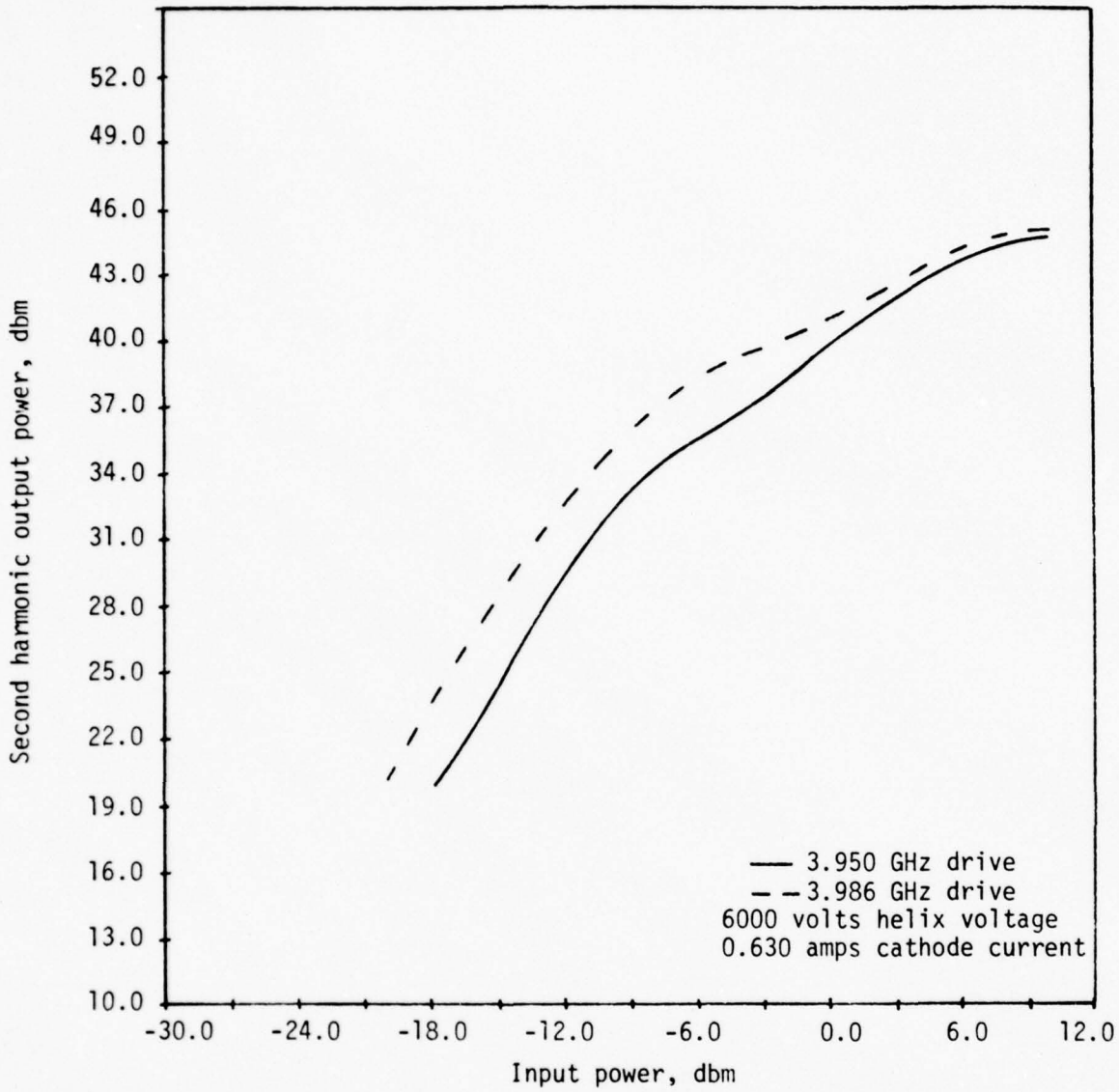

Figure 15c. Second harmonic output power vs. input power (driving at the fundamental) at two frequencies of interest. Solid line corresponds to input at 3.950 GHz, adjacent to but unaffected by the power hole. Dashed line corresponds to input at 3.986 GHz, the center of the power hole. At all points on both curves second harmonic output is at exactly twice the drive frequency.

The upper frequency power hole. Measurements of the type displayed in figures 14 and 15 were also performed at a helix voltage of 6600 volts where the upper frequency power hole predominates (see figure 10j). At the same beam current, the depth of this power hole is less than that of the lower frequency power hole (compare figures 10d and 10j). So a larger beam current is required to facilitate unambiguous measurements of power hole characteristics at this voltage. This introduces some difficulty in isolating the effects of the power hole and the drive-associated oscillation which both appear here as they did at a helix voltage of 6000 volts. At a cathode current low enough that the oscillation disappears, the power hole is too shallow for meaningful measurements. Also, the drive-associated oscillation and power hole occur at virtually the same drive frequency, in contrast to the situation apparent in figure 14. This further complicates isolation of the characteristics of the two phenomena.

Figures 16a, 16b, and 16c show fundamental output power, helix current, and second harmonic output power, respectively, vs. input power (driving at the fundamental) at two frequencies of interest. The solid curves correspond to input power at 4.072 GHz, adjacent to but unaffected by the power hole. These curves depict normal tube operation. The dashed curves correspond to input power at 4.092 GHz, the frequency of minimum fundamental output power for both the power hole and the drive associated oscillation. The curves illustrate deviations from normal tube operation associated with these phenomena. The interpretation of figure 16 is exactly the same as for figure 14, with the exception that in the latter, the power hole and drive-associated oscillation do not occur at the same drive frequency.

In figure 16c, the second harmonic output power associated with the oscillation is at precisely twice the drive frequency.

Figures 17a, 17b, and 17c display measurements taken at a lower cathode current (0.720 amps) than those in figure 16. The solid curves show normal tube operation at a drive frequency of 4.070 GHz, adjacent to but unaffected by the power hole. The dashed curves correspond to a drive frequency of 4.094 GHz, the frequency of both the power hole and drive associated oscillation. The oscillation, though still present at this cathode current, is less noticeable than in figure 16, and does not persist to as low an input power level. The interpretation of figure 17 is the same as for figure 15, and the conclusions based on comparison of figures 14 and 15 apply to figures 16 and 17 as well and will not be repeated here.

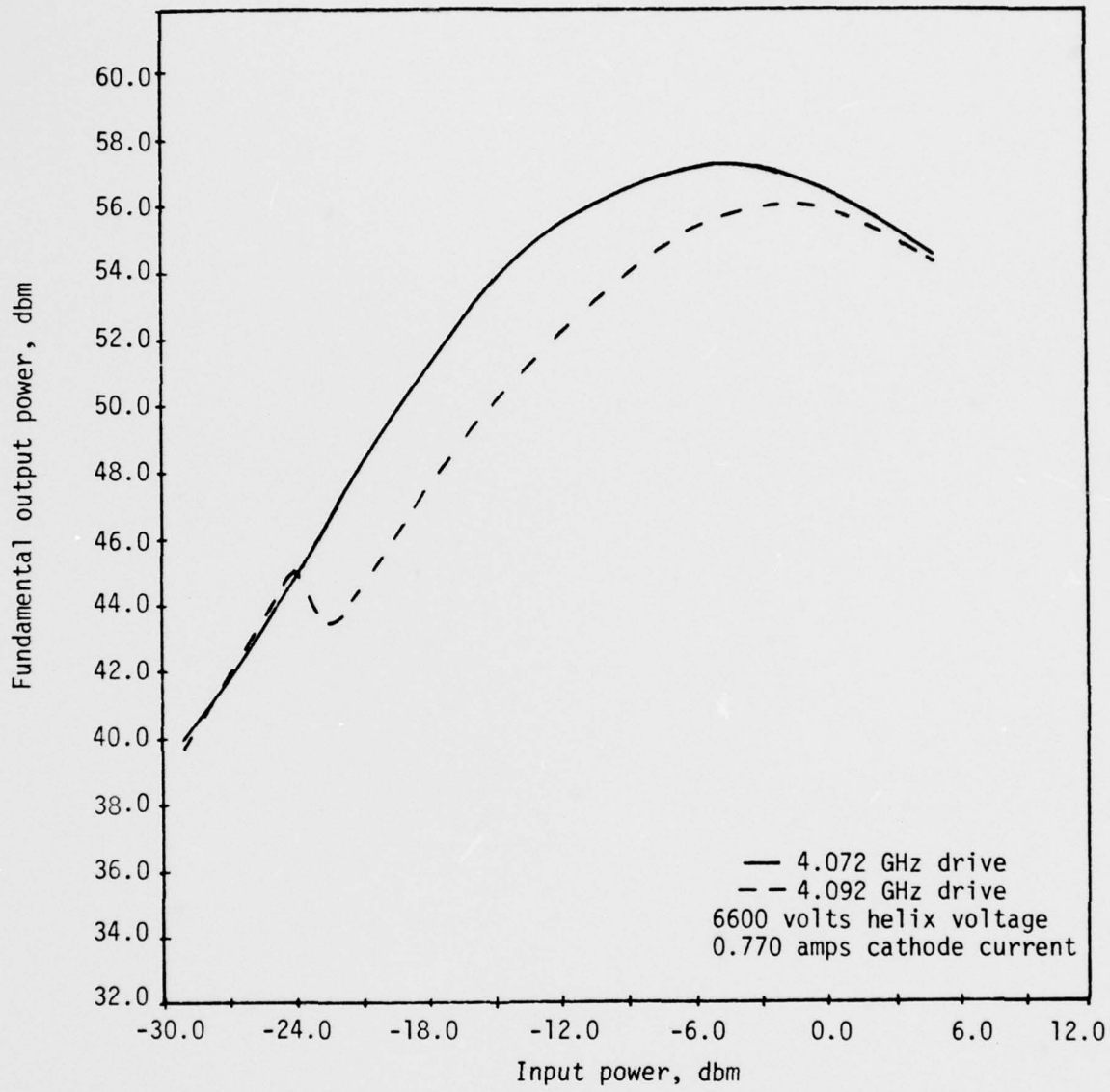

Figure 16a. Fundamental output power vs. input power (driving at the fundamental) at two frequencies of interest. Solid line corresponds to input at 4.072 GHz, adjacent to but unaffected by the power hole. Dashed line corresponds to input at 4.092 GHz, the center of the power hole and drive-associated oscillation.

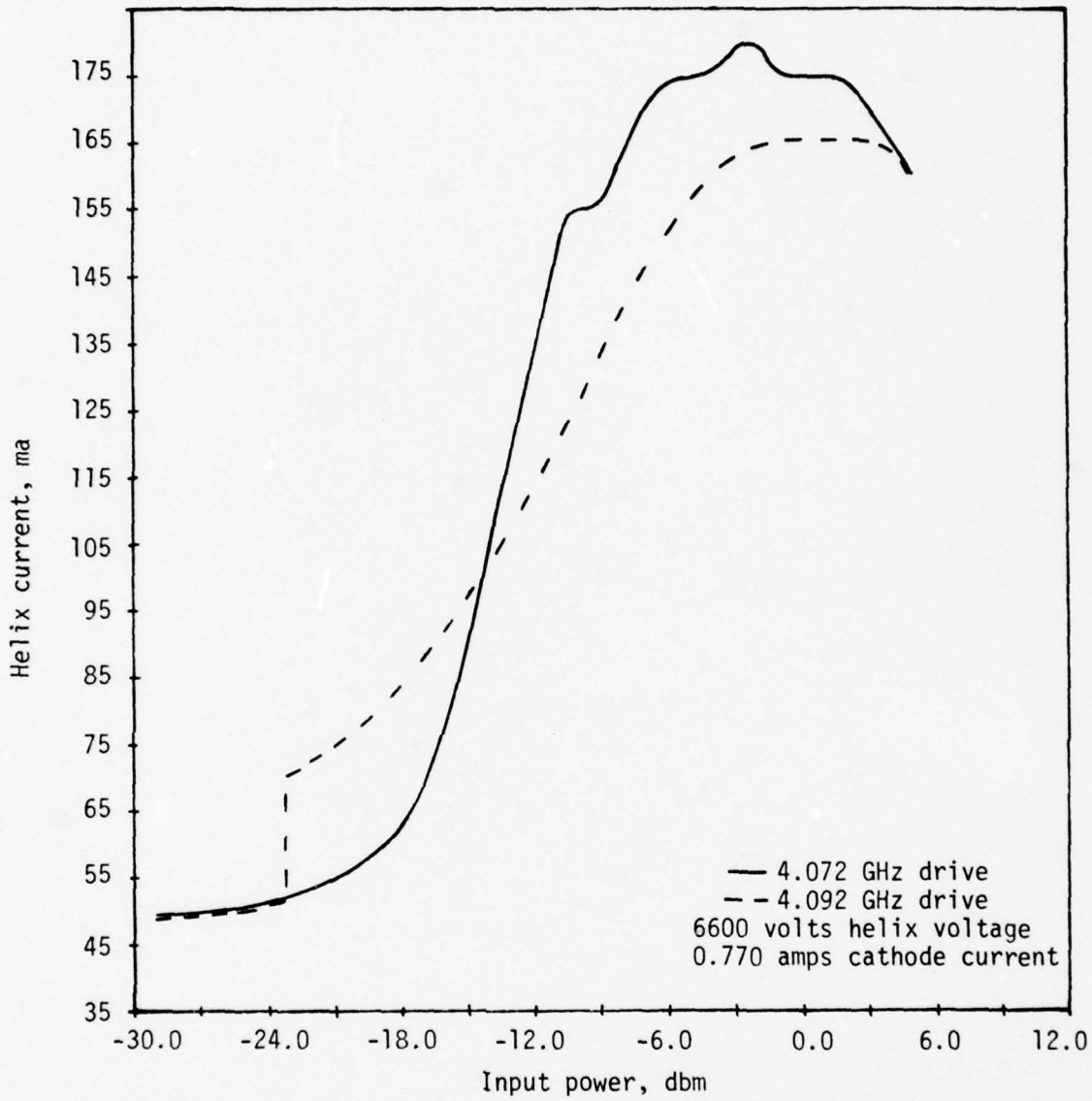

Figure 16b. Helix current vs. input power (driving at the fundamental) at two frequencies of interest. Solid line corresponds to input at 4.072 GHz, adjacent to but unaffected by the power hole. Dashed line corresponds to input at 4.092 GHz, the center of the power hole and drive-associated oscillation.

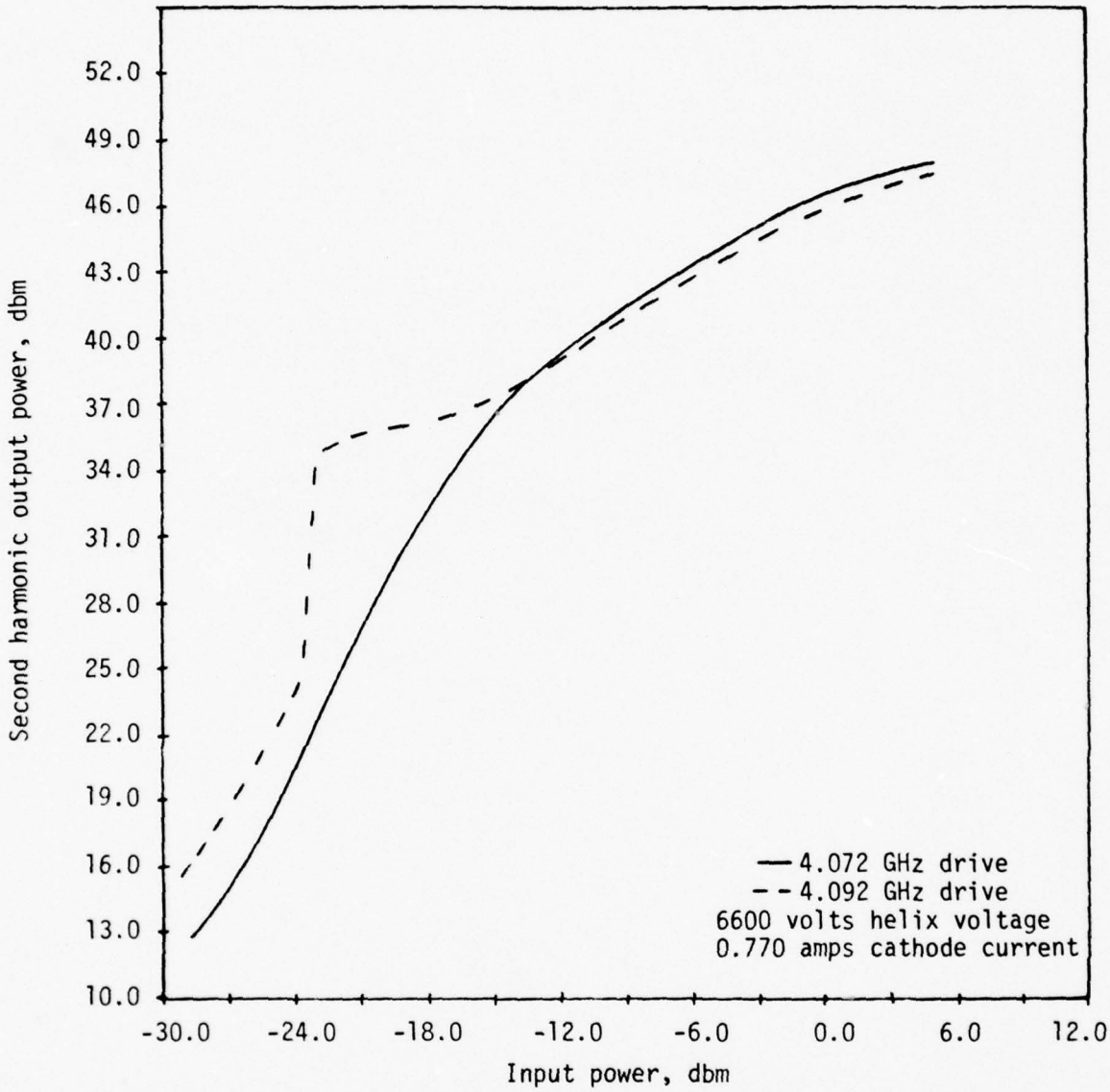

Figure 16c. Second harmonic output power vs. input power (driving at the fundamental) at two frequencies of interest. Solid line corresponds to input at 4.072 GHz, adjacent to but unaffected by the power hole. Dashed line corresponds to input at 4.092 GHz, the center of the power hole and drive-associated oscillation. At all points on both curves second harmonic output is at exactly twice the drive frequency.

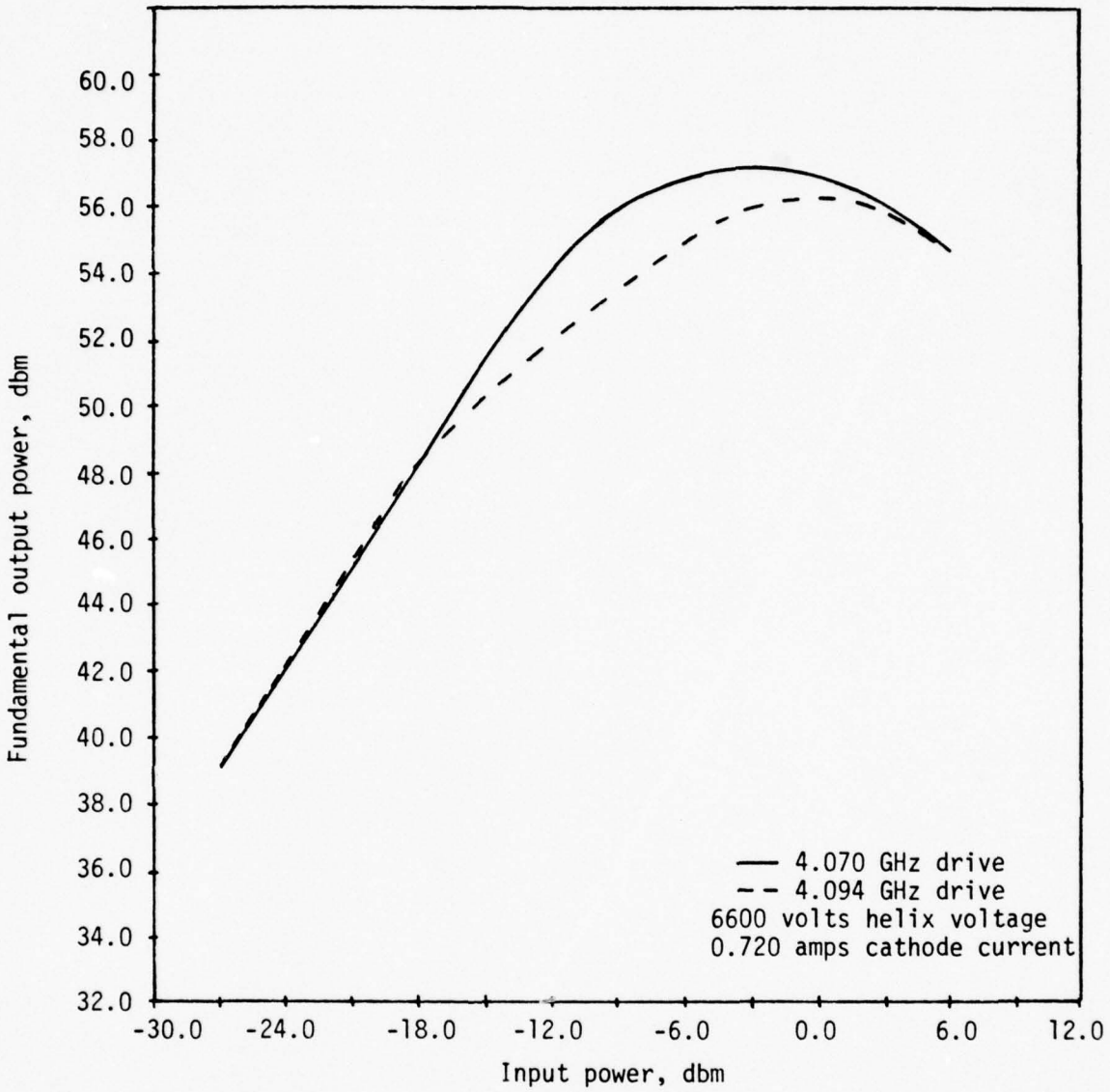

Figure 17a. Fundamental output power vs. input power (driving at the fundamental) at two frequencies of interest. Solid line corresponds to input at 4.070 GHz, adjacent to but unaffected by the power hole. Dashed line corresponds to input at 4.094 GHz, the center of the power hole and drive-associated oscillation.

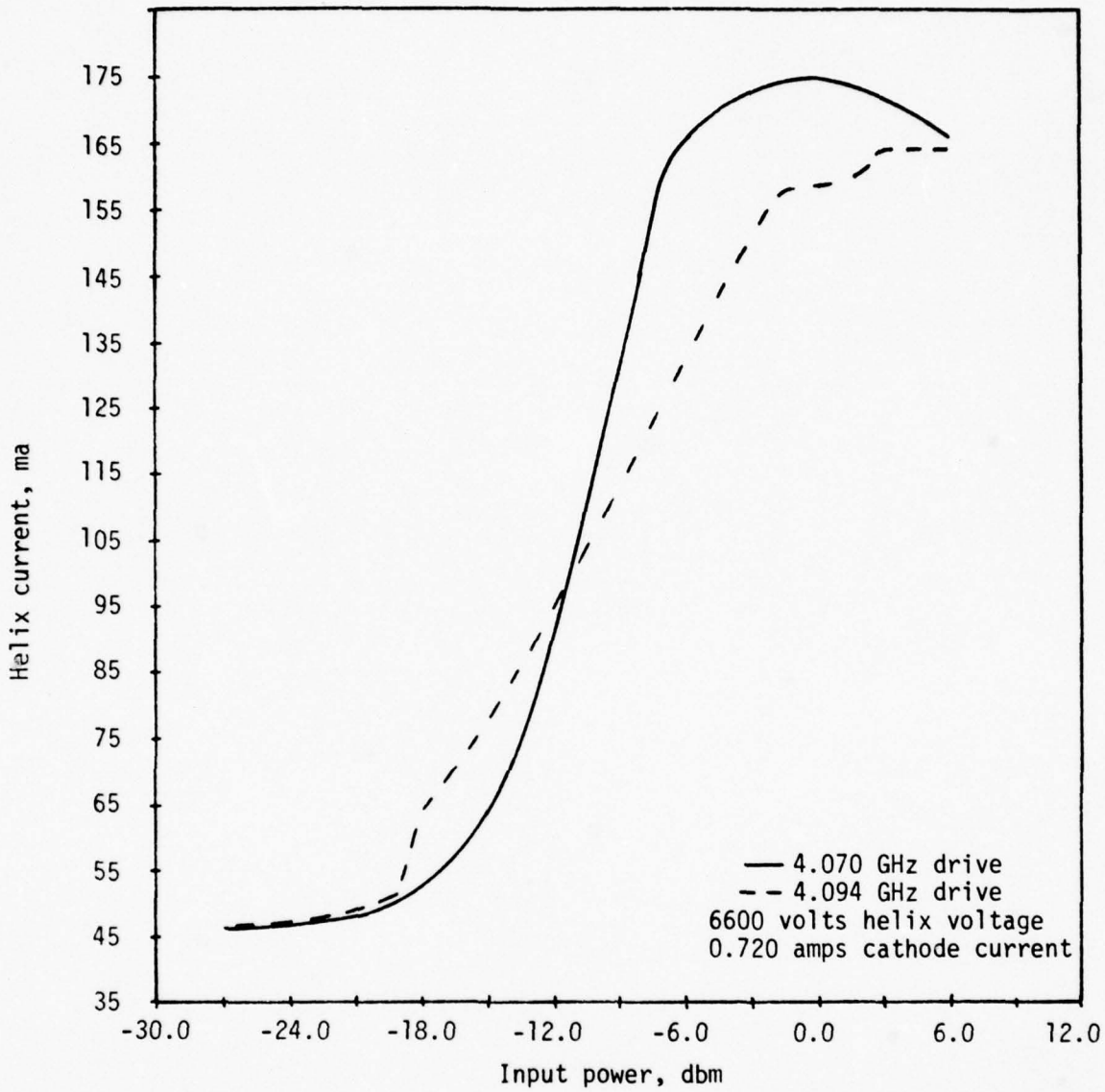

Figure 17b. Helix current vs. input power (driving at the fundamental) at two frequencies of interest. Solid line corresponds to input at 4.070 GHz, adjacent to but unaffected by the power hole. Dashed line corresponds to input at 4.094 GHz, the center of the power hole and the drive-associated oscillation.

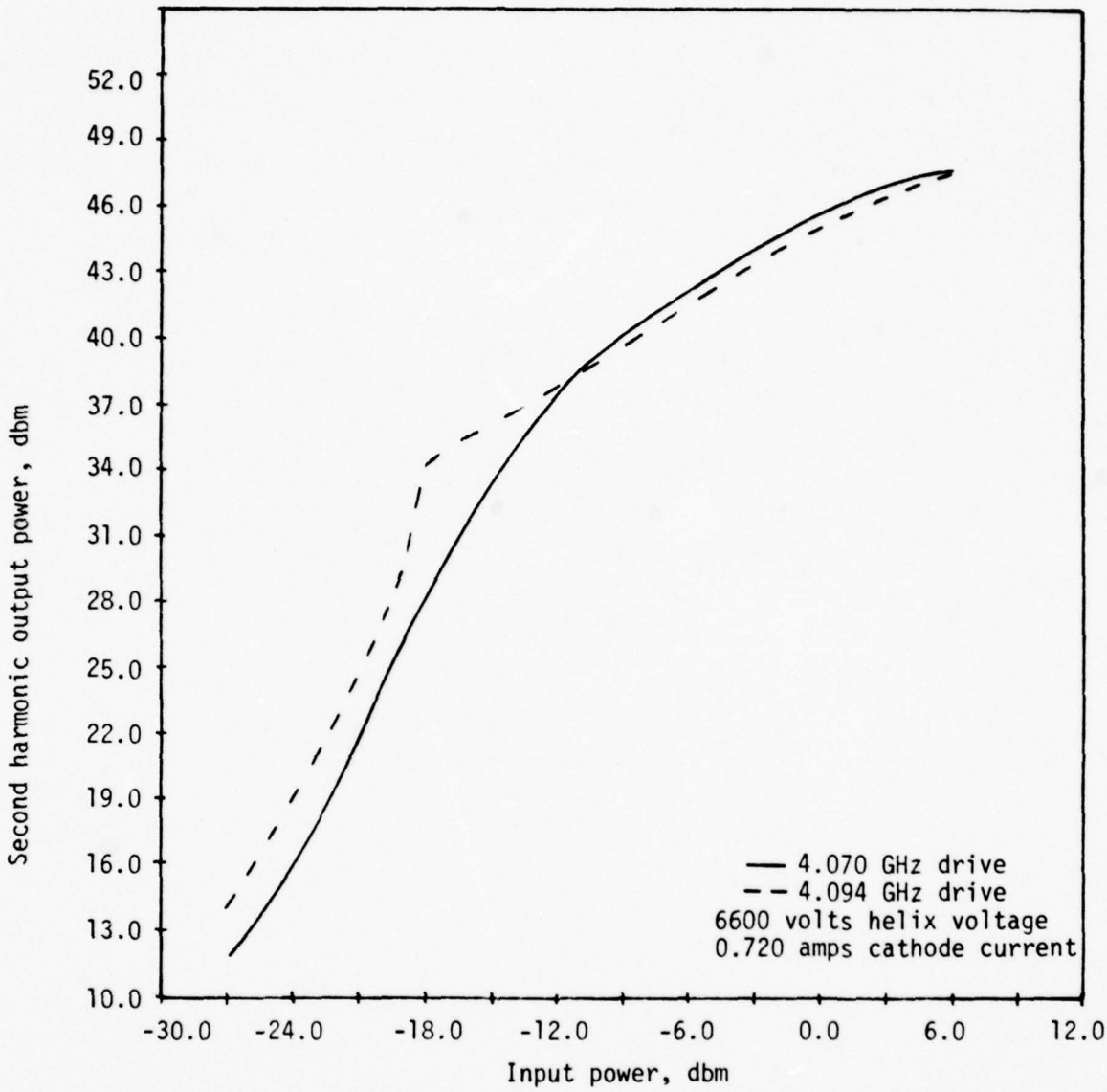

Figure 17c. Second harmonic output power vs. input power (driving at the fundamental) at two frequencies of interest. Solid line corresponds to input at 4.070 GHz, adjacent to but unaffected by the power hole. Dashed line corresponds to input at 4.094 GHz, the center of the power hole and drive-associated oscillation. At all points on both curves second harmonic output is at exactly twice the drive frequency.

Summary. The observations made in figures 14-17 may be briefly summarized by describing the two distinct effects. First, the power holes associated with power suck-out appear for input power within 15 db of saturation drive. The deficiencies present in fundamental output power and helix current (with input at the frequency of the power hole) correlate well and reach their largest value with input 10 db below saturation drive. They diminish as fundamental output power approaches saturation and disappear in overdrive. These deficiencies are measured relative to data taken while driving at a frequency adjacent to but unaffected by power suck-out. The second harmonic output power when driving at the frequency of the power hole exceeds that measured when driving at an adjacent frequency.

The second effect, the drive-associated oscillation, appears at considerably lower drive levels than the power holes. Associated with the narrow abrupt dip in fundamental output power at this frequency is a large increase in helix current and "second harmonic" output power, both with magnitude independent of input power. When input power or beam current is reduced below a threshold value required for oscillation, these symptoms abruptly disappear. The output power referred to as "second harmonic" is at the oscillation frequency which is not necessarily twice the drive frequency.

The measurements of this and the preceding section produce a clear picture of the appearance of power suck-out. In viewing these results, the implications of increased harmonic output power and the drive-associated oscillations lead back to the question posed preceding this report regarding the possible relationship

between power suck-out and the stop band measured in section III.A.1. Section III.A.4 proceeds with a careful consideration of this issue.

III.A.4 THE IMPORTANCE OF HARMONIC POWER IN THE APPEARANCE OF POWER SUCK-OUT

The nonlinear behavior of the electron beam leads to generation of harmonic output power in traveling-wave amplifiers.[12] Several of the measurements descrived so far suggest that this nonlinearity is important in the appearance of power suck-out. First, figures 14-17 reveal that the phenomenon is a large signal effect, present where the beam becomes nonlinear, and absent at low input power levels where non-linear effects are negligible. Second, associated with the power holes at the fundamental is an enhanced second harmonic output power, as seen in figures 13, 14c, and 15c. Third, in the drive-associated oscillation described in section III.A.3, output power appears near the second harmonic frequency (see figure 14c). Finally, power suck-out occurs in this WJ-3633-5 near half the stop band frequency, with the width of the stop band (measured in section III.A.1 as 140-180 MHz) approximately twice as large as the separation (80-90 MHz) of the two power holes which characterize power suck-out (see figure 10). This last observation suggests a harmonic relationship between the power holes and the edges of the stop band.

Correlation between a power hole and a gain peak near the stop band. The preceding comments provide motivation for investigating the behavior of this TWT with input power near the frequency of the stop band. Figure 18 displays the small signal gain of the tube in this frequency region. Helix voltage is 6100 volts; cathode current

is 0.700 amps; input power is sufficiently small that the TWT operates linearly, with gain independent of input power over the range of measurements. The two distinctive gain peaks in figure 18 (one at 8.009 GHz, the other at 8.130 GHz) appear at the boundaries of the stop band (8.07 ± 0.08 GHz) whose characteristics were discussed in section II and measured in section III.A.1. Between these peaks, the drastic reduction in gain gives further evidence of the presence of this stop band.

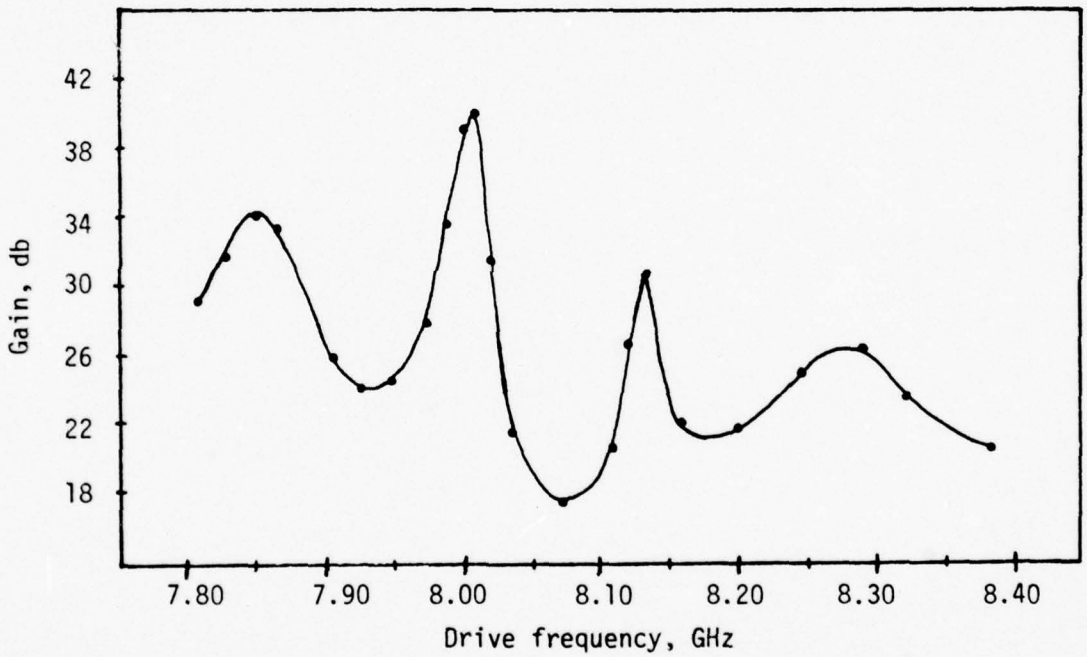

Figure 18. Small signal gain vs. drive frequency. Helix voltage is 6100 volts; cathode current is 0.700 amps.

Additional measurements, performed to determine the significance of the two gain peaks adjoining the stop band to power suck-out, reveal that the frequency of the gain peaks increases with helix voltage. Recall that the frequency of maximum power suck-out depends on helix voltage in the same way (see figure 101).

Also, the largest gain peak in figure 18 decreases in magnitude as helix voltage is tuned away from the voltage where it predominates, reminiscent of the behavior of the power holes (section III.A.1). Consequently, measurements were conducted to determine the dependence of the frequency and magnitude of the small signal gain peaks near the stop band on helix voltage and cathode current. Additional measurements determined the dependence of the frequency and depth of the power holes on the same two quantities.

A relationship was discovered between the gain peak at the lower edge of the stop band (which appears at 8.009 GHz in figure 18) and the lower frequency power hole of power suck-out (appearing in figure 10). Figures 19a and 19b show how the height of this gain peak, and the depth of this power hole vary with helix voltage (figure 19a) and cathode current (figure 19b). (Cathode current remains constant in figure 19a, while helix voltage remains constant in figure 19b.) The depth of the power hole clearly correlates with the height of the gain peak. At helix voltages and cathode currents where this gain peak predominates, the power hole is pronounced. And any change in helix voltage or cathode current which reduces the magnitude of the gain peak also diminishes the depth of the power hole. Furthermore, figures 20a and 20b display how the frequency of the gain peak and the frequency of the power hole vary with helix voltage (figure 20a) and cathode current (figure 20b). As in figure 19, the correlation is striking, with the frequency of maximum gain varying by less than 0.1 % from twice the frequency of the power hole. Note that the changes in helix voltage and cathode current alter the frequency of the gain peak by only tens

of megahertz, so that this peak always remains near the lower boundary of the output helix stop band. The data of figures 19 and 20 clearly demonstrate a relationship between power suck-out and the output helix stop band at pi radians phase shift per helix turn.

Attempts to correlate the upper frequency power hole of figure 18 to a gain peak at twice its frequency proved futile. As helix voltage is increased beyond the values used for figures 19 and 20, the gain of the TWT near the stop band decreases steadily. Consequently, at a helix voltage (6600 volts) where the upper frequency power hole predominates, noise and oscillations prevent measurements of small signal gain near the stop band. However, the gain peak seen at 8.130 GHz in figure 18 (6100 helix volts) near the upper edge of the output helix stop band suggests a correlation, since it appears near the second harmonic of the upper frequency power hole.

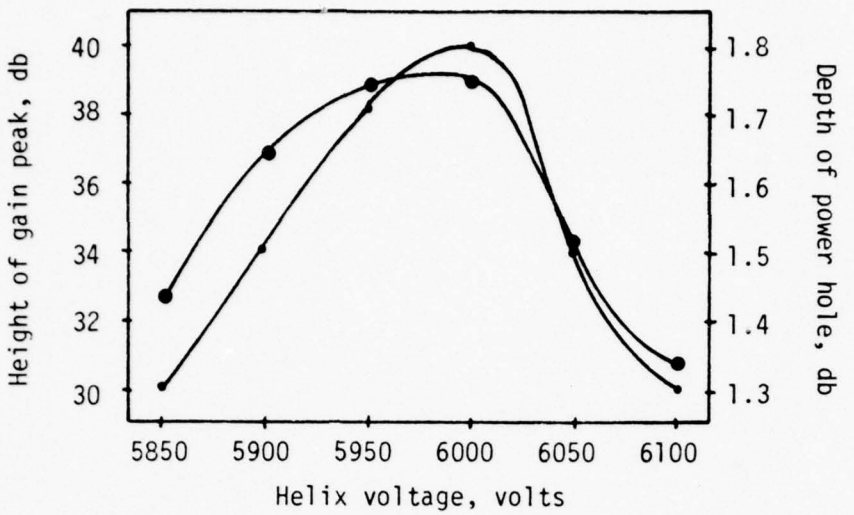

Figure 19a. Height of the gain peak (large dots) and depth of the corresponding power hole (small dots) vs. helix voltage. Cathode current is 0.650 amps.

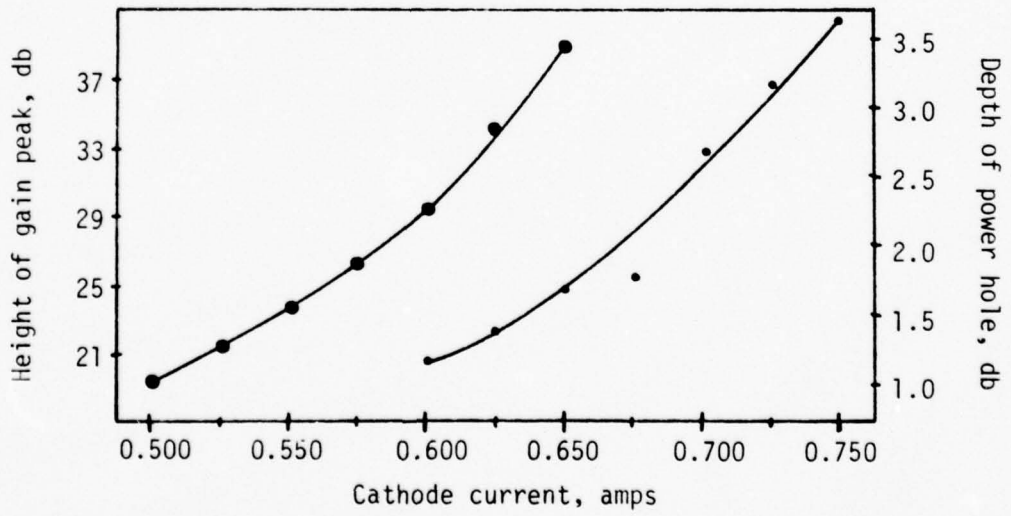

Figure 19b. Height of the gain peak (large dots) and depth of the corresponding power hole (small dots) vs. cathode current. Helix voltage is 6000 volts.

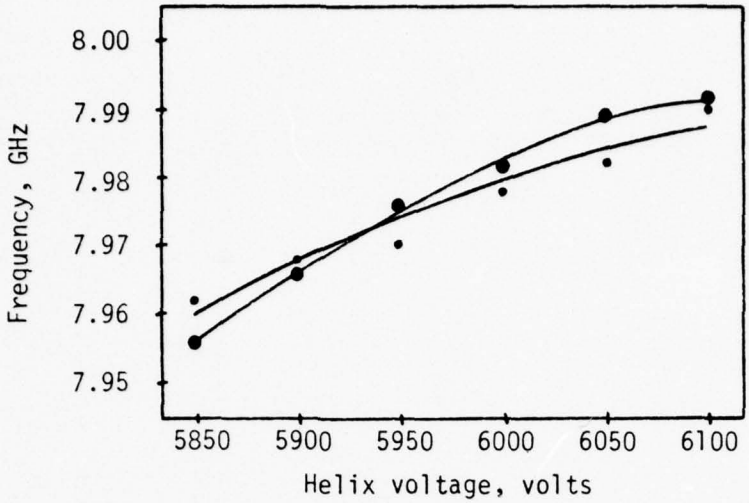

Figure 20a. Frequency of the gain peak (large dots) and twice the frequency of the corresponding power hole (small dots) vs. helix voltage. Cathode current is 0.650 amps.

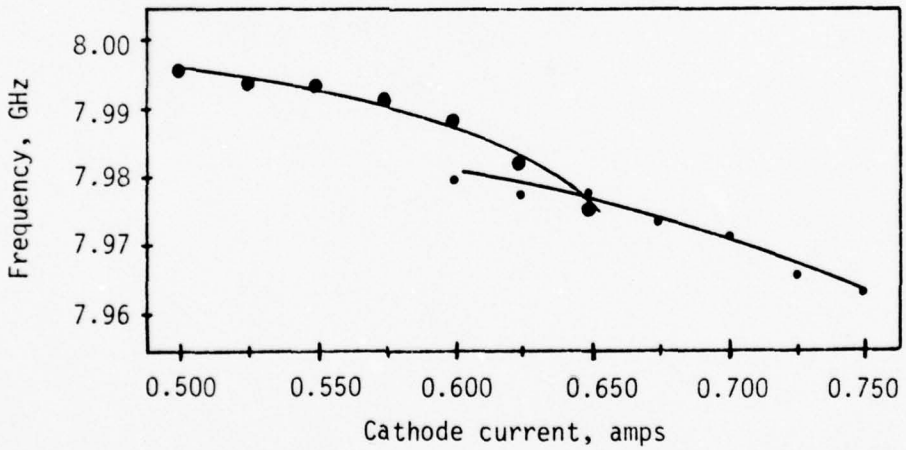

Figure 20b. Frequency of the gain peak (large dots) and twice the frequency of the corresponding power hole (small dots) vs. cathode current. Helix voltage is 6000 volts.

Drive-associated oscillations. In the vicinity of the gain peak at 8.009 GHz in figure 18, a sufficient increase in input power over the value used for the measurement of small signal gain induced oscillation. Figure 21 displays the threshold value of input power required to induce oscillation as a function of drive frequency, at the same helix voltage and cathode current as figure 18. The frequency of maximum gain in figure 18 coincides with the frequency where oscillation occurred with a minimum of input power. This oscillation at 7.994 GHz, independent of drive frequency, behaved in all respects like the drive-associated oscillation mentioned previously (section III.A.3). Further measurements similar to those in figures 18 and 21 indicate that the two phenomena are the same. The proper combination of cathode current and input power at

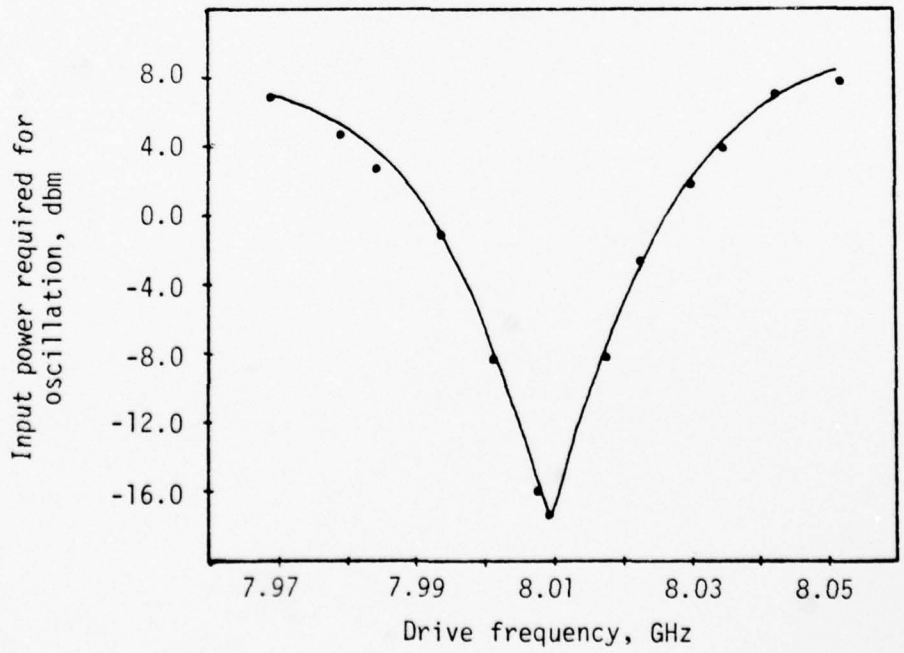

Figure 21. Input power required to induce oscillation vs. drive frequency, under the same operating conditions as figure 18.

the frequency of the gain peak in figure 18 induced an oscillation which could be duplicated with input at precisely one half the frequency of the gain peak. In the latter case, nonlinear beam behavior produced second harmonic power which induced the oscillation.

The lower frequency power hole and the drive-associated oscillation occuring in its vicinity have both been shown to be harmonically related to the gain peak at the lower boundary of the output helix stop band. Therefore, the presence of a drive-associated oscillation accompanying the upper frequency power hole gives further evidence of a harmonic relationship between the upper frequency power hole and the gain peak at the upper boundary of the output helix stop band.

Load dependence. Measurements similar to those in figure 18 revealed the sensitivity of the gain in this frequency range to load vswr. Any alteration of the attenuators, cables, and directional couplers comprising the output arm attached to the TWT resulted in different small signal gain characteristics. Figure 22 displays the small signal gain near the stop band vs. drive frequency at three different helix voltages; The curves differ significantly from figure 18 because of a change in output connections. Furthermore, the appearance of the power hole corresponding to the largest gain peak in figure 22 (at the lower boundary of the output helix stop band) reflects the fine structure of the gain peak which results from the load vswr. Further comments on this load sensitivity are delayed until section IV.

As a consequence of the above observation, the data of figures 19 and 20 were measured with output arm unchanged throughout.

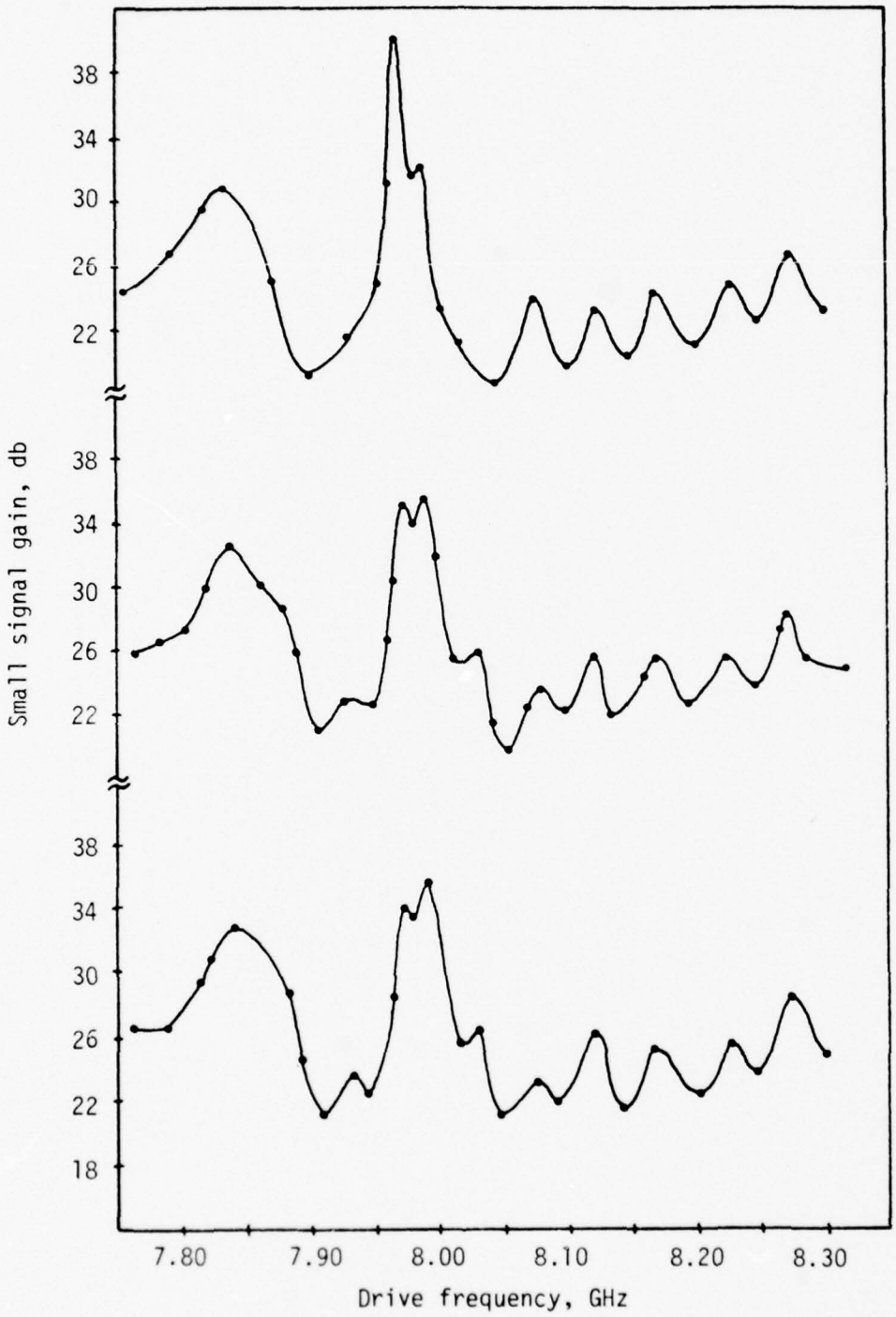

Figure 22. Small signal gain vs. drive frequency. Helix voltages are 5930, 6000, and 6025 volts for the top, middle, and bottom curves respectively. Cathode current is 0.670 amps throughout.

III.A.5 FINAL MEASUREMENTS ON THE WJ-3633-5

Presence of additional power holes. Section III.A.4 stresses the importance of second harmonic power in the occurance of power suck-out. In an attempt to influence the harmonic interaction, the TWT was driven near one half the stop band frequency with a low pass filter connected directly to its output. This filter permits all fundamental power to leave the TWT unaffected, but reflects all harmonic power back into the output helix section. Under these conditions, the deficiencies in fundamental output power and helix current at the suck-out frequency are enhanced. In all other respects, the power holes appear the same as without the low pass filter. Evidently, by preventing harmonic power from leaving the TWT, the low pass filter further inhibits the interaction at the fundamental frequency.

The preceding observation gives further evidence that power suck-out results from the interaction of second harmonic power at the stop band. This, along with previous results, suggests that power holes might appear at other frequencies which are harmonically related to the stop band frequency. Subsequent investigation revealed the presence of power suck-out at one third and one fourth the stop band frequency. These power holes behave in all respects according to the general description presented in section II.A.2, with drive induced oscillations accompanying power suck-out just as before. The power holes at these frequencies are less pronounced than those at one half the stop band frequency, but use of the low pass filter as described above increases the depth of these power holes, and aids in their identification. The following table lists the results

of measuring the frequency of the power holes at the helix voltages where they appear.

Helix voltage = 5950 volts;
Cathode current = 0.750 amps;

frequency of power holes, GHz	harmonic frequency, GHz
1.991	4th = 7.964
2.665	3rd = 7.995
3.981	2nd = 7.962

Helix voltage = 6650 volts;
Cathode current = 0.770 amps;

frequency of power holes, GHz	harmonic frequency, GHz
2.042	4th = 8.168
2.726	3rd = 8.178
4.095	2nd = 8.190

The frequencies are calculated to be harmonically related to the upper and lower boundaries of the stop band, as shown. The fourth, third, and second harmonics of the three power hole frequencies coincide to within 0.5%. The accuracy in measuring the frequency of the power holes, especially when they are shallow, could account for the discrepancies. The presence of these additional power holes suggests that any harmonic (not just the second harmonic) power interacting at the boundaries of the stop band region inhibits amplification at the fundamental frequency.

Harmonic injection. We return to consideration of the power holes at one half the stop band frequency, and continue in an attempt to influence the second harmonic interaction. The following measurements determine the effect of harmonic injection on power suck-out. Helix voltage, cathode current, fundamental input power, and frequency

are all adjusted to values where the power hole is pronounced. The fundamental frequency chosen (4.000 GHz) corresponds to the deepest point within the power hole. With these variables fixed, and with no second harmonic input power, the TWT produces 53.1 dbm fundamental output power, corresponding to a power hole 1.7 db in depth, with 76 ma helix interception current. Second harmonic input power sufficient to affect TWT operation is then introduced. The subsequent measurements of helix current, fundamental, and second harmonic output power as a function of relative phase of fundamental and second harmonic input power (with all other variables held constant) appear in figure 23. Figure 23c displays the expected behavior of second harmonic output power. When second harmonic input power adds in phase with the power generated by nonlinear beam behavior, the second harmonic output power achieves its largest value. But changing the phase of second harmonic input power by 180^{0} results in cancelation, and minimum second harmonic output power. Thus, as the relative phase of second harmonic input power sweeps through 360^{0}, second harmonic output power varies through a full cycle, from minimum to maximum to minimum, as in figure 23c. With second harmonic input power phased to produce maximum second harmonic output power, and hence maximum second harmonic fields within the TWT, fundamental output power (figure 23a) and helix current (figure 23b) reach their minimum values. Alternatively, with minimum second harmonic output power, fundamental output power and helix current achieve their largest values. This behavior supports the previous contention that in power suck-out, second harmonic fields within the TWT disrupt the interaction at the fundamental.

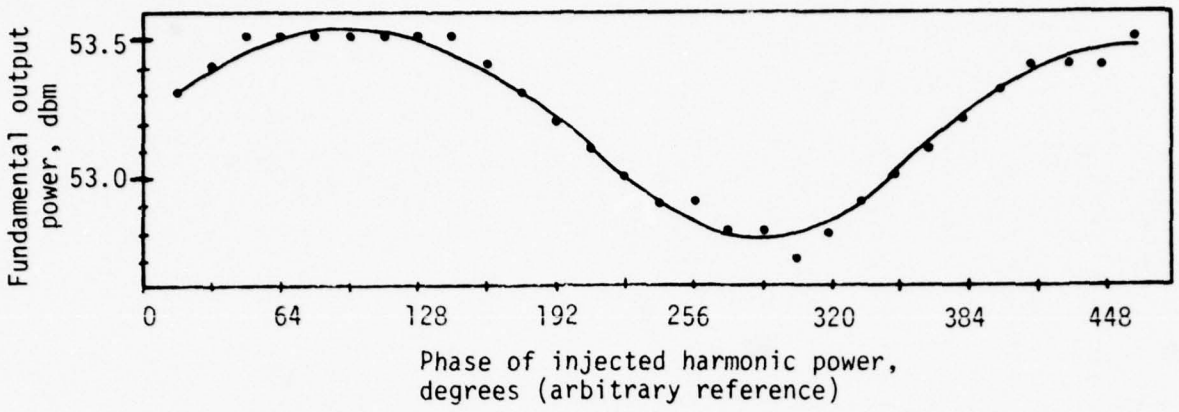

Figure 23a. Fundamental output power vs. phase of injected second harmonic power.

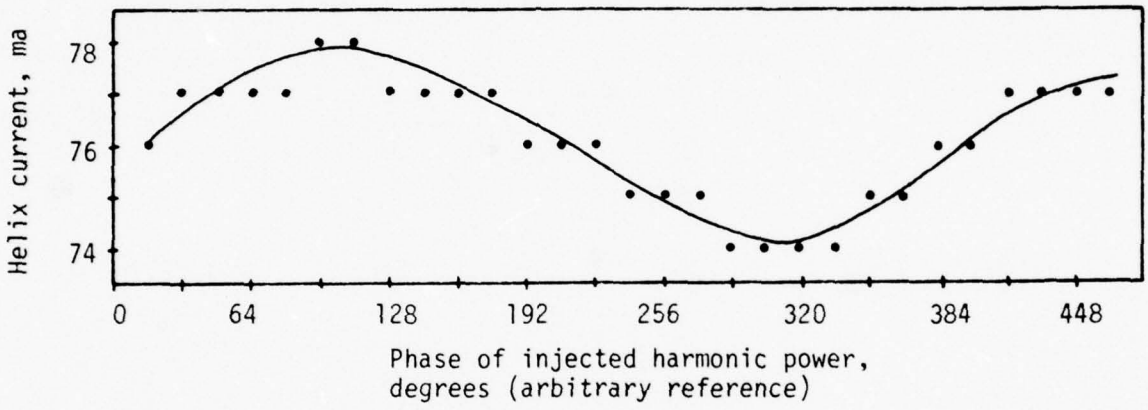

Figure 23b. Helix interception current vs. phase of injected second harmonic power.

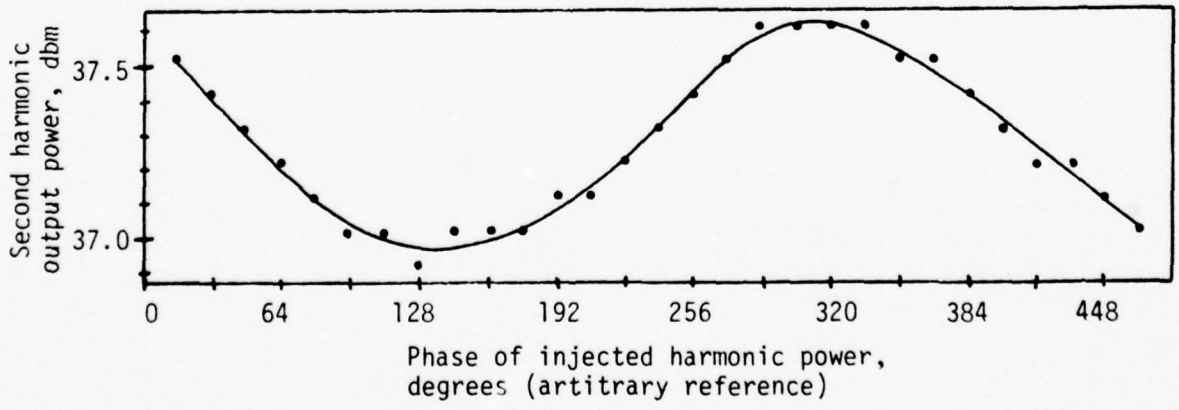

Figure 23c. Second harmonic output power vs. phase of injected second harmonic power.

Furthermore, a correlation is seen (in this tube) between the deficiencies in fundamental output power and helix current, as was first suggested in section III.A.2. But the results shown in figure 23 must be regarded with some caution. Injection of second harmonic power affects TWT behavior at all frequencies. Input of excessive power leads to oscillations and degrades performance. Also, the complexity of the experimental set-up increases the possibility of errors or misinterpretation of results. Therefore, these results have only limited value when viewed by themselves, and are best regarded as verification of previous measurements.

This completes investigation of the WJ-3633-5. All the measurements reported in section III.A were successfully duplicated to check their validity and preclude errors due to faulty equipment or carelessness. But in forming conclusions about power suck-out, one must recall that all this data derives from only one TWT. Section III.B addresses this limitation and extends the generality of the results presented in section III.A by investigating other traveling-wave amplifiers.

III.B. INVESTIGATION OF TWO WJ-3634-1 TRAVELING WAVE-AMPLIFIERS

As mentioned previously, the limited availability of operable traveling-wave amplifiers deterred attempts to establish the generality of the observations presented in section III.A. The only other functioning tubes found to be suitable for this study suffered from other defects, in addition to power suck-out, which hampered measurements. Consequently, section III.B contains only a brief investigation designed to reveal the salient features of power suck-out in two WJ-3634-1 TWT's, with the objective of verifying data from the

WJ-3633-5. Each of the two sections which follow discusses measurements on one of the WJ-3634-1 tube types.

III.B.1 WJ-3634-1, SERIAL NUMBER ONE

The output helix stop band. The presence of a stop band at pi radians phase shift per helix turn in the output section of this TWT is first established. (Data concerning the input helix stop band are omitted as in section III.A.1, since no relationship is found between this stop band and power suck-out.) The relevant measurements performed on the WJ-3633-5 were repeated on the WJ-3634-1.

For the output helix structure of the WJ-3634-1, measurements of wavelength along the helix axis at discrete excitation frequencies produced the data points displayed in figure 24* (compare to figure 7). For this helix wound at 12.16 turns per inch, a phase shift of pi radians per helix turn occurs for $1/\lambda = 2.39\ cm^{-1}$, corresponding to a frequency of 11.04 GHz as shown. Recall that the two space harmonics shown in figure 2 cross at this frequency, where a stop band results from misaligned dielectric helix support rods. Although the WJ-3634-1 output section is constructed with four dielectric support rods, the qualitative discussion of section II still applies.

As discussed previously (section III.A.1), indications of the presence of this stop band appear in measurements concerning oscillations induced in the absense of input power. The curves showing oscillation frequency (figure 25a) and start current (figure 25b) vs. helix voltage imply the presence of a stop band on

*As in section III.A.1, an output helix section identical to the one in the tube under test was used in this measurement; its use eliminated the necessity of dismantling the operable TWT.

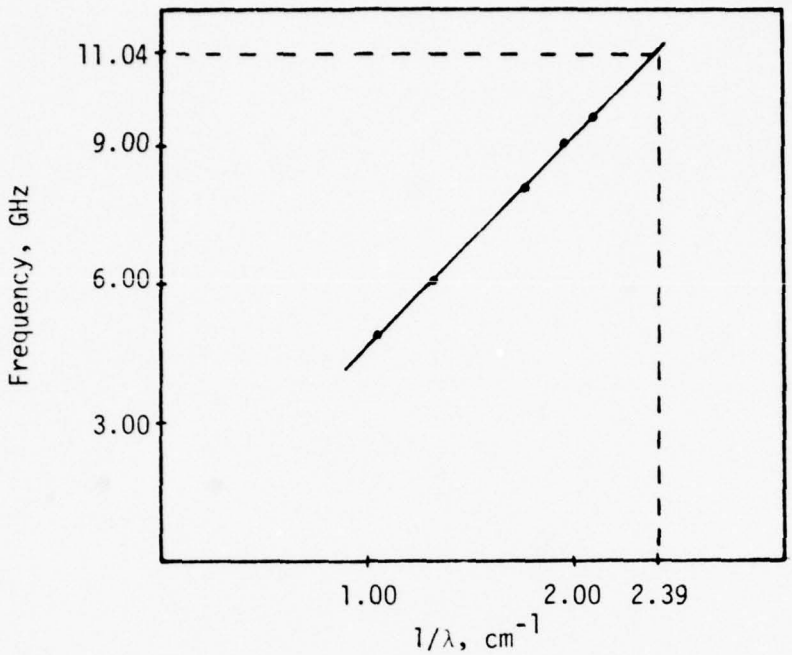

Figure 24. $1/\lambda$ vs. frequency on the (0) space harmonic for the output helix of the WJ-3634-1 TWT. The frequency corresponding to pi radians phase shift per helix turn is indicated. (The wavelength is measured along the axis of the helix.)

the output helix section with boundaries near 11.04 and 11.17 GHz (note the similarity to figure 8). In this case, the stop band is not severe, since oscillations occur within its boundaries (compare to the figure in the appendix).

The magnitude of the reflection coefficient looking into the output helix section can provide further information about the stop band (see section III.A.1). This data appears in figure 26 for the WJ-3634-1, but its interpretation in terms of the stop band is ambiguous.

Measurements of the crossover frequency, output helix oscillations without input power, and reflection coefficient provide compelling indications of a stop band present at pi radians phase shift per helix turn in the output section of the WJ-3633-5 (see section III.A.1).

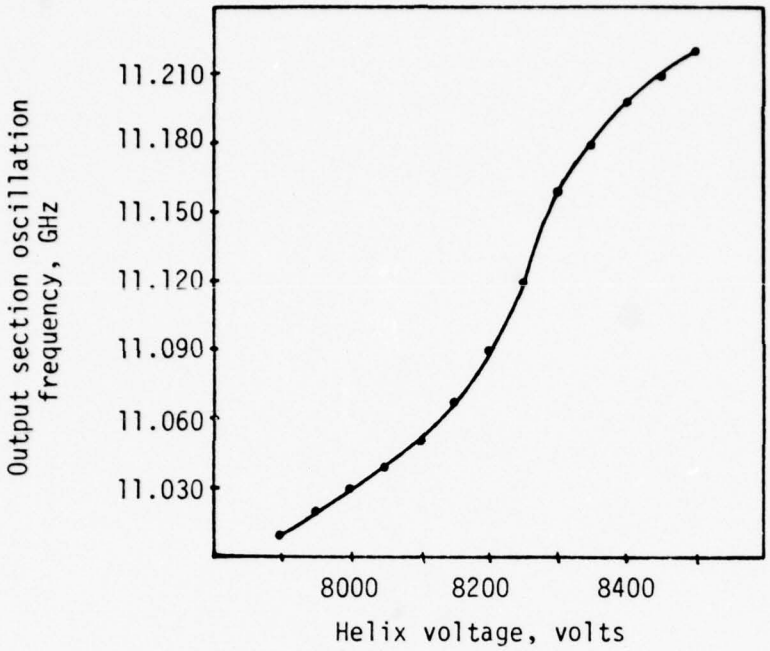

Figure 25a. Oscillation frequency vs. helix voltage for the output section of the WJ-3634-1.

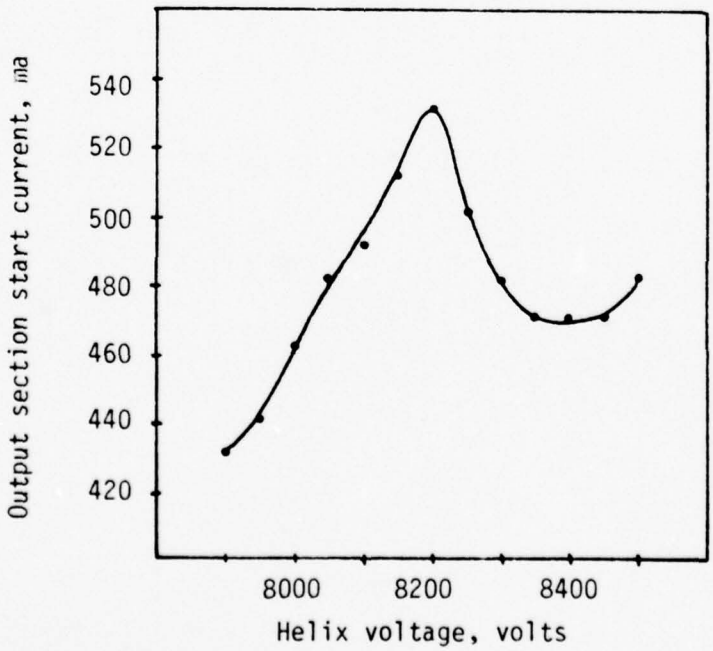

Figure 25b. Output section start current vs. helix voltage corresponding to the measurements in figure 25a.

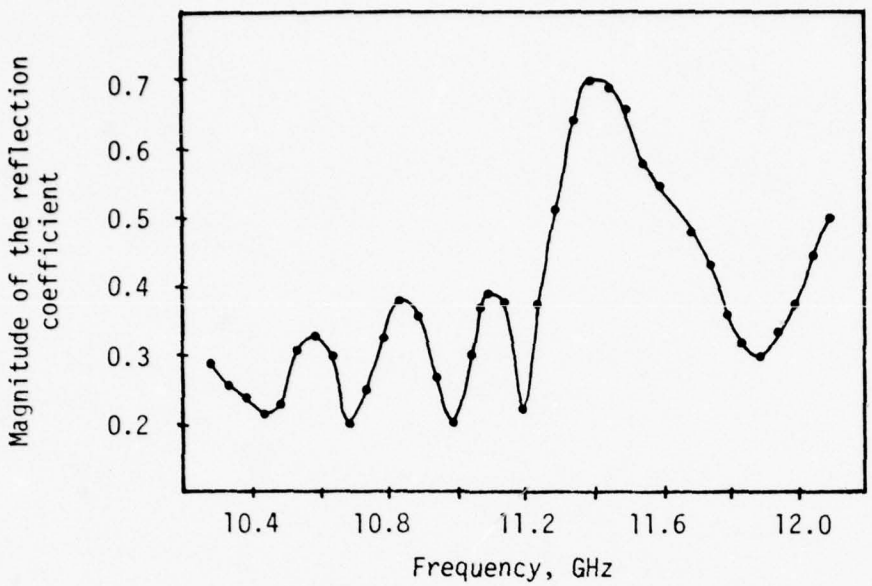

Figure 26. Magnitude of the reflection coefficient vs. frequency looking in the output of the WJ-3634-1.

However, the corresponding measurements performed on this WJ-3634-1 produce less certain results. Section II explains some of the problems associated with locating this type of stop band, hence the difficulty encountered here is not unexpected. While it seems likely from figure 25 that a stop band is present, conclusions based on this result should be carefully qualified.

Characteristics of power suck-out. The behavior of this WJ-3634-1 is complicated by a strong load dependence, which affects the gain peaks near the stop band, the power holes, and also the substantial gain variations present within the bandwidth of the TWT, as well. This prevents certain measurements concerning power suck-out, since all conventional choices of output arm produce power holes whose complex appearance impairs easy characterization. (This complex appearance involves many narrow,

abrupt, closely spaced dips.) Only with a low pass filter (which transmits the fundamental but reflects all harmonics) attached to the output of the TWT do the power holes take on a simple appearance, similar to those in figures 10d or 11d. All subsequent measurements were performed with the low pass filter, so no attempt was made to establish a correlation relating the power holes to the gain peaks near the stop band for this TWT. Nevertheless, substantial gain peaks were observed in the vicinity of the stop band.

As expected, two power holes appear near one half the stop band frequency. Their bahavior as a function of helix voltage, cathode current, and input power confirms the observations discussed in section III.A.2. The depth of these power holes is considerably larger (8.5 db at maximum) than observed for the WJ-3633-5. Consequently, both power holes appear at a single helix voltage, as shown in figure 1 (which derives from another WJ-3634-1).

As before, power holes also appear at one third and one fourth of the crossover frequency. The frequency of maximum power suck-out within the power holes appears below.

Helix voltage = 8150 volts;
Cathode current = 0.700 amps;

frequency of power holes, GHz	harmonic frequency, GHz
2.750	4th = 11.000
2.795	4th = 11.180
3.664	3rd = 10.992
3.727	3rd = 11.181
5.500	2nd = 11.000
5.589	2nd = 11.178

The lower frequency power hole of each pair has a harmonic near 11.000 GHz, while the upper frequency power hole of each pair has a harmonic near 11.180 GHz. These harmonics of the power holes

(which coincide to within 0.1%) appear very close to the frequencies (11.04 GHz and 11.17 GHz) indicated as boundaries of the stop band by the oscillation measurements of figure 25. This corroborates the observations in section III.A.5.

The last observation involves the helix interception current associated with power suck-out in this WJ-3634-1. In contrast to the situation for the WJ-3633-5 (see figures 14b and 15b), when driving at the frequency of the power hole, helix current is greater than at adjacent frequencies. This increase in helix current is largest under conditions where the power hole predominates, and vanishes when the power hole is absent. No drive-associated oscillations occured in this tube, so this behavior of the helix current results entirely from power suck-out. A discussion of the implications of this observation appears in section IV.

III.B.2 WJ-3634-1, SERIAL NUMBER TWO

Investigation of the second WJ-3634-1 produced results very similar to those in section III.B.1. Therefore, only a brief discussion accompanies this section.

The output helix stop band. For this traveling-wave amplifier, the input section oscillates at a lower beam current than the output section preventing any measurements, such as those shown in figures 8 or 25, concerning the stop band. Figure 27 displays the magnitude of the reflection coefficient looking into the output section as a function of frequency; the data seems to indicate a stop band between 11.45 and 11.80 GHz. This is noticeably higher than the crossover frequency predicted by figure 24, or the stop band frequency derived from figure 25. But these two TWT's were

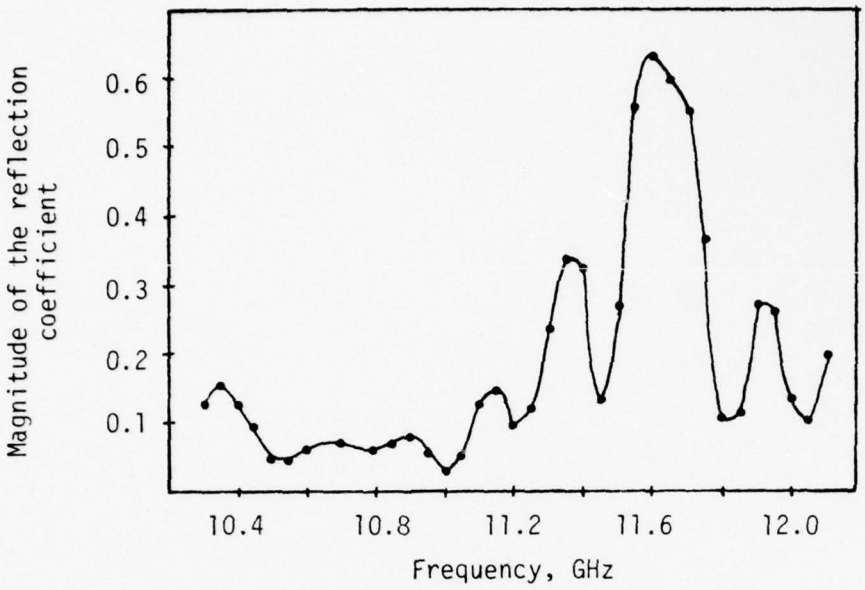

Figure 27. Magnitude of the reflection coefficient vs. frequency looking in the output of the WJ-3634-1.

constructed several years before their use here, and the lack of complete documentation hindered the accurate determination of quantities such as helix pitch. Therefore, acknowledging the possibility of minor internal differences between these TWT's, power suck-out in WJ-3634-1 serial number two was investigated with this limited knowledge of the output helix stop band at pi radians phase shift per turn.

Characteristics of power suck-out. Substantial gain variations and strong load dependence affect the behavior of this WJ-3634-1, as was the case in section III.B.1. The power holes appear much the same for both TWT's; therefore, for the same reasons discussed in section III.B.1, all measurements were performed with the low pass filter connected to the TWT output. The frequencies of maximum power suck-out in the power holes present in this WJ-3634-1 are listed.

Helix voltage = 8150 volts;

Cathode current = 0.550 amps;

frequency of power holes, GHz	harmonic frequency, GHz
2.862	4th = 11.448
3.818	3rd = 11.454
3.915	3rd = 11.745
5.720	2nd = 11.440
5.870	2nd = 11.740

Oscillations interfered with the measurements near 2.9 GHz, so only one power hole could be identified there. The lower frequency of each pair has a harmonic near 11.45 GHz, while the upper frequency of each pair has a harmonic near 11.74 GHz. These two harmonic frequencies compare favorably with the boundaries of the stop band predicted by figure 27, providing further support for observations in section III.A.5. In contrast to the situation in section III.B.1, a deficiency in helix current accompanies the power holes as was the case for the WJ-3633-5 (see figures 11d and 15b). But because of problems with oscillations, no further measurements were performed on WJ-3634-1 serial number two.

IV. SUMMARY AND CONCLUSIONS

Section III contains a detailed account of a variety of measurements performed with the objective of thoroughly and systematically characterizing power suck-out. Section IV.A presents a cumulative description of the phenomena concentrating on power suck-out, with only a brief reference to the drive-associated oscillations discussed in section III.A. Section IV.B proposes a qualitative model which attempts to explain the prominent features of power suck-out.

IV.A SUMMARY OF THE RESULTS

The results reviewed here derive primarily from one WJ-3633-5 high power single helix dual mode amplifier which operates near 6000 helix volts with 0.7 amps cathode current. Data from two WJ-3634-1 TWT's (presented in section III.B) corroborates these results, allowing the observations to be generalized beyond application to one particular device.

The axial periodicity of a helical conductor in free space determines features of the propagation characteristics. But the design and construction of practical helix slow wave structures creates additional periodicities which affect propagation. In particular, a stop band appearing at pi radians phase shift per helix turn results from the periodicity commonly introduced by imperfect alignment of dielectric helix support rods.

Power suck-out, characterized by two adjacent power holes in the fundamental output of the TWT, occurs at one half the stop band frequency of the output helix. The power holes typically have a bandwidth of 0.5% with depth, which depends strongly on operating parameters, ranging up to 5 db. An increase in

cathode current significantly enhances the phenomenon so that it is most troublesome in dual mode ECM TWT's. To each power hole there corresponds a helix voltage for maximum depth. The helix voltage where the lower frequency power hole predominates is less than the helix voltage where the upper frequency power hole predominates. Any change away from these "optimum" helix voltages results in a decrease in the depth of the corresponding power hole. (A change of ±5% in helix voltage essentially eliminates the power hole.)

Furthermore, the frequency of maximum power suck-out varies with helix voltage and cathode current. For the WJ-3633-5, an increase in helix voltage causes the power hole frequency (approximately 4.0 GHz) to increase at 60 kHz/volt, while an increase in cathode current causes the power hole frequency to decrease at 60 kHz/ma. Both power holes exhibit the same dependence so that their separation remains constant, independent of cathode current and helix voltage.

Comparisons made between TWT operation with input at the frequency of the power hole and with input at an adjacent frequency (unaffected by the power hole) reveal the characteristics of power suck-out as deviations from normal amplifier behavior. Both power holes display the same dependence on input power, so the following description applies to either at the appropriate values of helix voltage and cathode current where that particular power hole is pronounced. At small signal input levels, the phenomenon is absent. Not until fundamental input power is within 15 db of saturation drive does the power hole begin to appear. As input power is

increased in the WJ-3633-5, the deficiency in fundamental output power grows, reaching its maximum value 10 db below saturation drive. This deficiency decreases with higher input power levels, and the power hole eventually disappears with the TWT slightly overdriven.

The helix interception current accompanying the power hole deviates from the value at adjacent frequencies. The magnitude of this deviation correlates with the depth of the power hole, exhibiting the same dependence on helix voltage, cathode current, and input power. But while an increase in helix current appears with the power holes in one TWT, a decrease accompanies them in another. (We emphasize that the change in helix interception current discussed here results from power suck-out, and not from the drive-associated oscillation which appears under certain conditions at essentially the same frequency as each power hole.)

For all levels of input power, the second harmonic output power reaches a maximum value with input at the frequency of the power hole. The magnitude of the enhanced second harmonic output power is insufficient to account for most of the power "missing" at the fundamental (in the power hole). Neither can the second harmonic gain peak alone explain the power hole at fundamental, since harmonic gain peaks appear at other frequencies with no corresponding power hole in the fundamental. The power holes occur only under specific conditions, one of which requires that substantial harmonic power is present near the frequency of the output helix stop band at pi radians phase shift per helix turn.

Distinctive gain peaks appear when driving the TWT near the frequency of the output helix stop band. One substantial gain

peak occurs at the lower boundary of the stop band at precisely the second harmonic of the lower frequency power hole of power suck-out. At helix voltages and cathode currents where this gain peak predominates, the power hole is pronounced. Any change in helix voltage or cathode current which reduces the magnitude of this gain peak correspondingly diminishes the depth of the power hole. And the frequency of the gain peak varies with helix voltage and cathode current in a way that maintains the precise second harmonic relationship with the power hole. The output helix stop band is therefore clearly involved in the occurrence of power suck-out.

In addition, power suck-out also occurs at one third and one fourth of the output helix stop band frequency, with the power holes similar in appearance to (though less pronounced than) those which occur at one half the stop band frequency. At both of these lower frequencies, the behavior of the two adjacent power holes in fundamental output as a function of helix voltage, cathode current, and input power coincides with the description given above. The power holes occuring at the lower frequency in each pair have a common harmonic at the lower edge of the stop band, while the power holes corresponding to the upper frequency in each pair have a common harmonic at the upper edge of the stop band.

This concludes the summary of the experimental description of power suck-out accomplished in this report. Specific data contained in section III quantitatively supports each of the characteristics described above. While confirming some of the observations which preceded the investigation (listed in the introduction), this report corrects some and establishes a more thorough, precise description of the phenomenon.

IV.B A PROPOSED MODEL TO EXPLAIN POWER SUCK-OUT

Section IV.B now attempts to interpret and interrelate the results presented in section IV.A within a self-consistent theory.

The substantial gain variations which appear at frequencies above the designed bandwidth of the TWT (figure 18) have been discussed by Cohen[13]. Due to poor output match within the TWT at these frequencies (figure 9), a considerable fraction of the power incident on the output connection is reflected back onto the output helix section. As this reflected power propagates toward the input of the tube, any discontinuity will cause an additional reflection. Such reflections might occur at the sever between input and output helix sections. Thus, the twice reflected signal returns to the TWT output, and the round trip phase shift determines its relationship to the original signal. For frequencies where the round trip phase shift is an even multiple of pi, signals add in phase at the output and maximum gain results. And for frequencies where the round trip phase shift is an odd multiple of pi, the signals cancel at the output and minumum gain occurs. Note that based on this interpretation, at a frequency of maximum gain, standing waves appear on the output helix section, while much smaller fields are present at a frequency of minimum gain. Also, the dependence of propagation constant on frequency determines the spacing between gain peaks, while the height of the gain peaks depends on the round trip gain (or loss) of the reflected signal.

Recall that changes in helix voltage and cathode current alter the propagation constants for the hot circuit. Consequently, within this model, the frequency of maximum gain, where round

trip phase shift is an even multiple of pi, is expected to depend on helix voltage and cathode current. Such behavior was observed in section III.A.4 (figures 20a and 20b). This explanation of the gain peaks also accounts for their load dependence (compare figures 18 and 22), since any change in the output connection will affect the internal reflections which generate these gain variations.

To continue developing the model, we examine the effect of a stop band in the output helix section on the behavior of the gain peaks. As discussed in section II, the characteristic low group velocity near the boundaries of the stop band results in high interaction impedance at these frequencies. Thus, we expect enhanced gain peaks to appear at the boundaries of the stop band under certain operating conditions. Attenuation accompanies propagation within the stop band (section II, figure 6) so gain in this region is expected to be low. Figure 18 displays all these features: two substantial gain peaks separated by an abrupt minimum appear at the stop band frequency measured in section III.A.1.

According to this model, any change in helix voltage which displaces the frequency of the gain peak away from the region of low group velocity (and high interaction impedance) should diminish its magnitude; the data in figure 19a support this conclusion. (The small changes in helix voltage along the abscissa of the figure do not significantly affect the synchronism between circuit and slow space-charge waves.) However, both forward and backward wave interactions can occur near the stop band, where the proper synchronism exists between the slow space-charge wave and both forward and bachward circuit wave phase velocities. Also, the

behavior of the stop band complicates any analysis, so little can be said about the spacing of the gain peaks, or even the mechanism of gain involved at these frequencies. Nevertheless, the model successfully explains the presence of enhanced gain peaks at the boundaries of the stop band, and predicts that large standing wave fields on the output helix section will accompany amplification at the frequency of these gain peaks.

With these considerations in mind, consider TWT operation under conditions where a gain peak appears at one boundary of the stop band with its characteristic high interaction impedance. With input power at one half the frequency of the gain peak, under small signal conditions, the beam behaves linearly and normal amplification occurs. But increased input power produces nonlinear beam behavior resulting in harmonic power within the tube. Then, according to previous assumptions, the gain peak at second harmonic produces large standing wave fields in the output helix section as well as enhanced second harmonic output power. These second harmonic fields on the output section affect the electron beam: longitudinal fields disturb the bunching process essential for amplification at the fundamental, and radial fields defocus the beam. The combined effects of the second harmonic fields in the output helix section inhibit the interaction at the fundamental producing the power hole characteristic of power suck-out.

This model is consistent with the results of section III. As shown in figure 14a, the power hole appears only at input power levels which produce nonlinear beam behavior. Furthermore, the lower frequency power hole occurs at precisely one half the frequency

of the enhanced gain peak at the lower boundary of the stop band (figure 20). The depth of the power hole correlates with the magnitude of this gain peak, showing identical dependence on helix voltage and cathode current (figure 19). This last observation clearly indicates that the power hole occurs only under operating conditions where the gain peak is pronounced. And power holes appear at other frequencies which have harmonics at either boundary of the stop band (page 65). Finally, the results of the experiment on harmonic injection emphasize the importance of harmonic fields in producing power suck-out (figure 23).

As a consequence of the model proposed here, we can interpret the change in helix interception current which accompanies power suck-out (figure 14b). (We again emphasize that the deviation in helix current under discussion results from power suck-out, not from the drive-associated oscillation discussed earlier.) Two opposing effects determine the behavior. First, since amplification at the fundamental disturbs electron trajectories, the reduction in fundamental output in the power hole tends to reduce the helix interception current. But the harmonic fields which inhibit the interaction at the fundamental defocus the beam and increase helix current. The overall change in helix current in a particualr TWT depends on which effect dominates, as determined by various properties such as the quality of beam focus, the ratio of average beam radius to helix radius, or the magnitude of harmonic fields. Thus, the behavior of helix current associated with the power hole will vary between TWT's, a dip in current appearing in one device, but a peak in helix current occuring in another, as was

observed in section III.

The qualitative model presented in this section attempts to explain power suck-out in a manner which is compatible with the results of section III. This discussion supplements the experimental investigation of the phenomenon by providing a plausible interpretation for the various results. For simplicity, the intuitive model proposed here avoids the complexity of a thorough analysis. However, since further conclusions cannot be justified without a more rigorous theory, this completes the experimental characterization of power suck-out undertaken in this report.

V. RECOMMENDATIONS FOR DESIGN AND FURTHER STUDY

The first half of section V suggests research to continue this investigation. The report concludes in section V.B with discussion of design consideration to reduce power suck-out.

V.A FURTHER STUDY

The measurements described in sections III and IV provide a firm basis for a theoretical solution to power suck-out. The development of a comprehensive theory which goes beyond simple elaborations of the model in section IV requires computer analysis. A conventional large signal program could be modified to include the effect of the stop band (at pi radians phase shift per helix turn) on the harmonic fields. Clearly, a careful consideration of helix propagation at frequencies near the stop band is needed.

Additional measurements might investigate the effect of various design parameters, such as helix tape width or oscillation suppression techniques, on the appearance of power suck-out. In particular,

more information is needed to understand what determines the depth of the power holes. Comparison of measurements performed before and after physical changes in a particular TWT would provide useful design information. For example, one might evaluate the effect of shifting the alignment of a helix support rod on characteristics of the stop band and power suck-out. Finally, an examination of the spent electron beam entering the collector should indicate some aspects of the interaction producing power suck-out.

V.B DESIGN

As suggested before this report (see introduction), the output helix stop band at pi radians phase shift per helix turn plays a significant role in power suck-out. This observation indicates that careful construction techniques which avoid introducing the stop band should suppress the phenomenon. Efforts to improve the output match near the stop band frequencies would reduce the gain peaks associated with the power holes (section III.A.4) further inhibiting power suck-out. The load vswr at the output helix stop band should also be minimized. Unfortunately, these design recommendations are difficult to enact. Nevertheless, recalling the importance of harmonic power to power suck-out (section III.A.4), it is expected that by greatly attenuating all harmonic power, the phenomenon can be eliminated. The lossy, resonant meander lines deposited on helix support rods, as designed by Varian Associates (discussed by C. E. Hobrecht[14]), introduce such attenuation and should consequently effectively control power suck-out.

APPENDIX: EXPERIMENTAL SET-UPS AND EQUIPMENT

This appendix discusses measurement techniques, equipment, and resulting limits of accuracy to supplement the data of section III.

In this study, the traveling-wave amplifiers are operated on a Universal Voltronics power supply (for helix voltage, collector voltages, grid voltages, cathode current, and filament voltage and current). The TWT operating parameters important to this investigation are monitored as follows. The helix voltage (relative to cathode) is measured on a digital voltmeter accurate to within 1%. Due to the linear behavior of the voltage divider in this meter, the voltage changes involved in the measurements displayed in figures 101, 19a, or 20a are also known to this accuracy, with a precision of one volt. A pearson Electronics pulse current transformer (toroid) determines cathode current with less than 5% error. Once again, the characteristics of this device allow measurement of changes in cathode current (which is the important quantity in the results) involved in figures 19b or 20b to the same accuracy, with a precision of 10 ma. Helix interception current passes through a resistor and measurement of the voltage drop determines this current with an accuracy of 5%.

The following list summarizes the equipment used for the measurements discussed section III.

Narda Microwave:	directional couplers
	variable attenuators
	co-axial phase shifter
	slotted line impedance meter

Hewlett Packard:	sweep oscillators crystal detectors co-axial to rectangular waveguide adapters frequency meters 8742A reflection test unit (2.0-12.4 GHz) 8411A harmonic frequency converter 8410A network analyzer 8414A polar display 7044A x-y recorder 415E SWR meter
Weinschel Engineering:	attenuators
Tektronix:	7403 oscilloscope
General Microwave:	454A thermoelectric power meter
Microlab:	FXR / low pass filter

Two of the components listed above impose important limits on experimental results. The thermoelectric power meter permits measurement of microwave power at a single frequency accurate to within 0.1 db. Frequencies can be determined within 10^6 Hz (0.001 GHz) by the Hewlett Packard frequency meter. We now proceed to describe the use of this equipment for obtaining the results of section III.

The configuration for measuring fundamental output power and second harmonic output power as a function of input power (at discrete frequencies), helix voltage, and cathode current appears in figure 28. Beginning at the input arm, we briefly explain the set-up. The low pass filter following the sweep oscillator removes all harmonics from the input signal. The variable attenuator adjusts the level of input power, which is measured with thermo-electric power meter #1. D.C. filters on the TWT input and output eliminate undesired ground paths for the helix interception current.

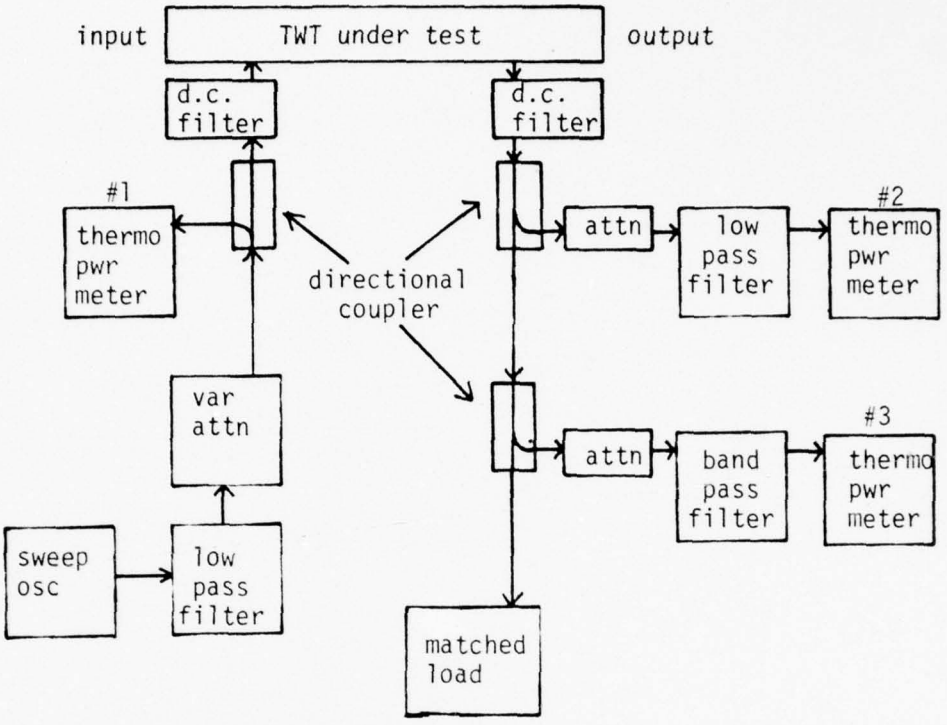

Figure 28.

A low pass filter on the first auxilary output arm eliminates all harmonics, allowing measurement of fundamental output power on power meter #2. The band pass filter in the second auxilary output arm consists of a low pass filter and a length of rectangular waveguide (high pass filter) which combine to pass only the second harmonic output power, which is then measured on power meter #3. Frequency meters inserted before each power meter determine the various frequencies. For swept frequency measurements, crystal detectors with oscilloscopes (giving faster response time) replace the thermoelectric power meters.

Harmonic injection (see section III.A.5) is performed with the configuration shown in figure 29. As in the preceding paragraph,

AD-A067 916 VARIAN ASSOCIATES INC PALO ALTO CA F/G 9/1
AN INVESTIGATION OF POWER SUCK-OUT IN HELIX TRAVELING-WAVE TUBE--ETC(U)
DEC 78 D P HINSON F49620-77-C-0102
UNCLASSIFIED AFOSR-TR-79-0392 NL

2 OF 2
ADA
067916

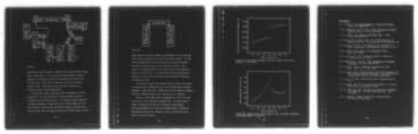

END
DATE
FILMED
6-79
DDC

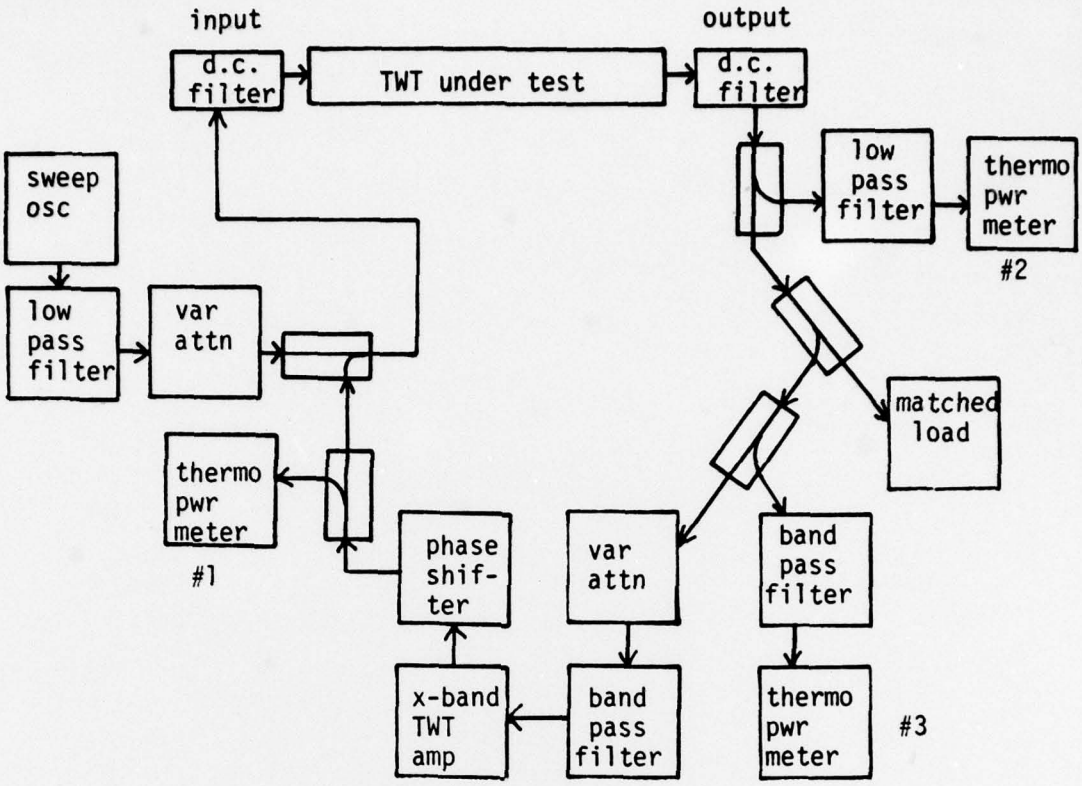

Figure 29.

power meters #2 and #3 measure fundamental and second harmonic output power, respectively. In this case, the second harmonic output is adjusted in amplitude and phase and injected at the input of the TWT under test. Power meter #1 monitors the level of injected harmonic power. The various filters and their functions are identical to those described previously.

Oscillations without input power were investigated as follows (figure 30). At a particular helix voltage, cathode current is increased until oscillation occurs. The frequency meters determine oscillation frequency. Output section oscillations appear only at the TWT output; input section oscillations appear at the TWT input, and are carried onto the output section by the electron beam, as well.

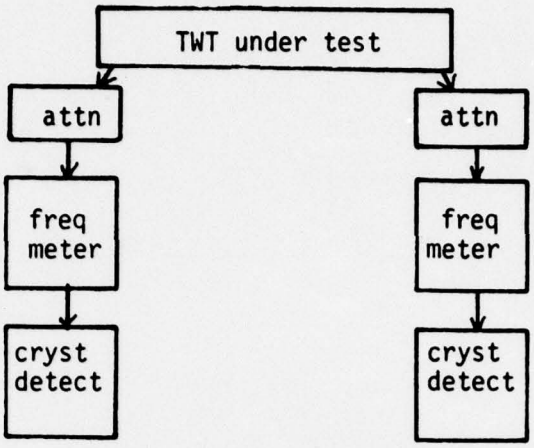

Figure 30.

Hence, output oscillations cannot be investigated if the associated start current exceeds the input oscillation start current. For this reason, complete data of start current and oscillation frequency are usually available only for the input helix section. Such results are displayed below for the input section of the WJ-3633-5 studied in section III.A.1. The two figures clearly indicate the presence of a stop band; these results are provided for comparison to figures 8a and 8b.

The reflection coefficient looking into the output helix section is measured with a standard set-up of the following Hewlett-Packard equipment: sweep oscillator, reflection test unit, harmonic frequency converter, network analyzer, polar display, and x-y recorder.

Finally, a small metal bead is suspended on a nylon line along the helix axis (of a partially assembled TWT). The bead reflects signals introduced onto the helix, producing standing waves. Using the SWR meter and slotted line impedance meter to determine wavelength at a particular frequency results in dispersion curves such as the one in figure 7.

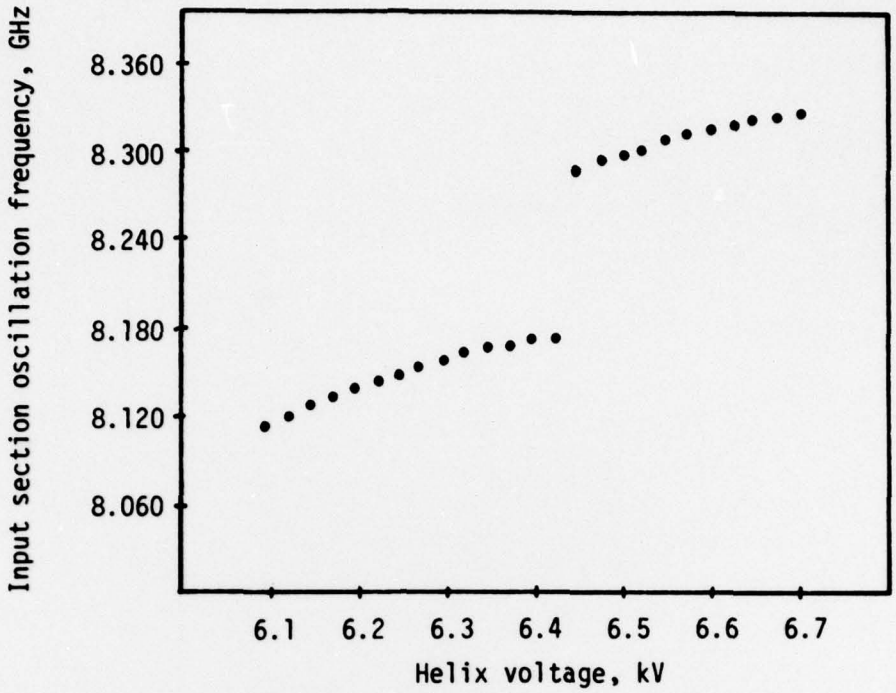

Figure 31a. Oscillation frequency vs. helix voltage for the input section of the WJ-3633-5.

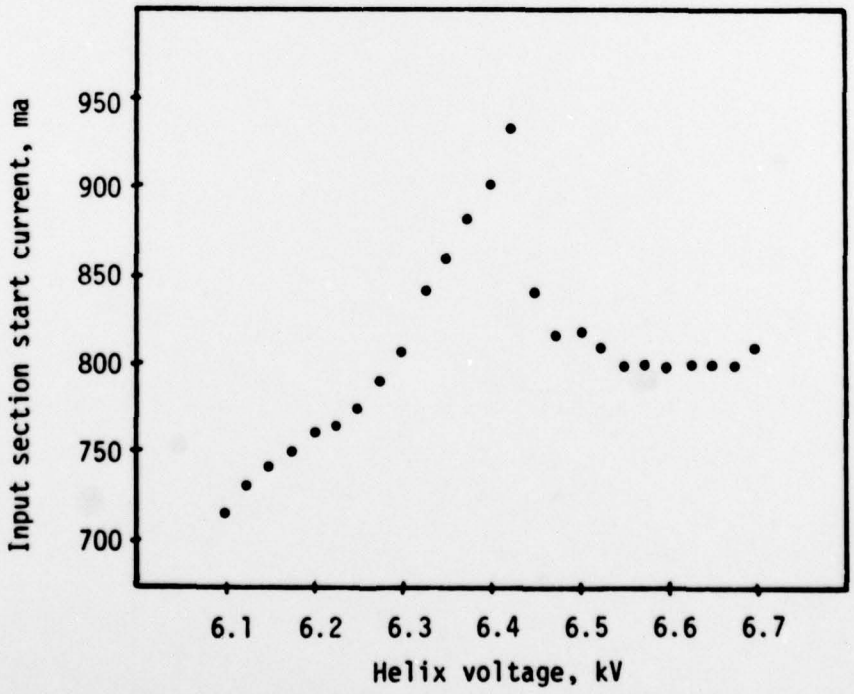

Figure 31b. Input section start current vs. helix voltage corresponding to the measurements in figure 31a.

BIBLIOGRAPHY

1) L. Brillouin, 1946, Wave Propagation in Periodic Structures (New York: McGraw-Hill).

2) J.W. Gewartowski and H.A. Watson, 1965, Principles of Electron Tubes (Princeton, N.J.: Van Nostrand).

3) J.F. Gittins, 1964, Power Traveling-wave Tubes (London: English Universities).

4) G. Dohler and R.R. Moats, Sept. 1977, "IBCFA Attenuator for Improved Stability", report #AFAL-TR-77-134, Northrup Corp.

5) S. Sensiper, May 1951, "Electromagnetic Wave Propagation on Helical Conductors", Tech. Report No. 194, R.L.E., M.I.T.

6) D.A. Watkins, 1958, Topics in Electromagnetic Theory (New York: Wiley).

7) J.R. Pierce, Feb. 1954, "Coupling of Modes of Propagation", J. Appl. Phys., 25, 179-183.

8) M. Chodorow and C. Susskind, 1964, Fundamentals of Microwave Electronics (New York: McGraw-Hill).

9) J.R. Pierce, "Theory of Beam-type Traveling-wave Tube", Proc. I.R.E., 35, 111-123 (1947).

10) J.A. Ruetz, 1958, "Microwave Interaction of Electron Beams and Non-propagating Periodic Structures", Tech. Report No. 30 (project 204), Stanford Electronics Laboratories.

11) E. Lien, July 1978, "Monterey Revisited", Microwave Journal, 21, 7.

12) F. Paschke, June 1957, "On the Nonlinear Behavior of Electron-beam Devices", RCA Review, 221-242.

13) S.A. Cohen, Jan. 1957, "Traveling-wave Tube Gain Fluctuations with Frequency", IRE Trans. on Electron Dev., ED-4, 1, 70-78.

14) C.E. Hobrecht, "Monterey Revisited", Microwave Journal, 21, 7, pg. 23, July 1978.